EPJ manuscript No.
(will be inserted by the editor)

A Theoretical Study of the Magnetically Deformed Inner Crust Matter of Magnetars

Arpita Ghosh and Somenath Chakrabarty†

Department of Physics, Visva-Bharati, Santiniketan, India 741 235
†E-mail:somenath.chakrabarty@visva-bharati.ac.in

Received:January 16, 2013 / Revised version: date

Abstract. We have studied various physical properties of magnetically deformed atoms and the associated matter, replacing the atoms by the deformed Wigner-Seitz (WS) cells at the crustal region of strongly magnetized neutron stars (magnetars). A relativistic version of Thomas-Fermi (TF) model in presence of strong magnetic field in cylindrical coordinates is used to study the properties of such matter.

PACS. 97.60.Jd Neutron stars – 71.70 Landau levels – 26.60.GJ Neutron star crust – 26.69.Kp Equation of State of neutron-star matter

1 Introduction

From the observational evidence of a few strongly magnetized neutron stars, which are supposed to be the sources of anomalous X-rays and soft gamma rays, also called magnetars [1,2,3,4], the study of the effect of strong magnetic field on dense neutron star matter, including the crustal matter, both outer crust and inner crust regions of such compact stellar objects have gotten a new dimension. These exotic objects are also called anomalous X-ray pulsars (AXP) and soft gamma repeaters (SGR). The outer crust of a typical neutron star in general, is mainly composed of dense crystalline metallic iron [5]. The density of the upper edge of such metallic crystalline matter is $\sim 10^6 - 10^7$gm cm^{-3}, whereas the bottom edge is $\sim 10^{11}$gm cm^{-3}, the matter consists of nuclei (also some highly neutron rich nuclei), surrounded by cylindrically deformed distribution of electron gas, makes the system electrically charge neutral and drifted out free neutrons, if the density of matter is $\geq$ neutron drift value. Since the density is high eneough, it is therefore absolutely impossible to investigate the properties of such matter in material science laboratories, even at zero magnetic field. The observed surface magnetic field of the magnetars is $\sim 10^{15}$G, which is again too high to achieve in the terrestrial laboratories. Also, it is quite possible that the interior field of such exotic objects can go up to $\sim 10^{18}$G (which can be shown theoretically by virial theorem). If the magnetic field at the interior is really so high, then most of the physical and chemical properties of dense neutron matter should change significantly from the conventional neutron star (radio pulsar) scenario (see the recent article by one of the co-authors [6] for necessary references). In [6], the matter in the outer crust region of strongly magnetized neutron stars have been studied using Thomas-Fermi approximation, in which the WS cells are assumed to be spherical in nature and arranged in a regular manner to form dense crystal of metallic iron ($\sim$ BCC-type). Even though the magnetic field strength at the crustal region is slightly higher than 10^{15}G, it must change significantly most of the properties of dense matter, both in the outer crust and the inner crust regions of the magnetars [6,7]. It is believed that strong magnetic field can cause a structural deformation of the metallic atoms (see e.g., [8]) present in the inner crust region of a neutron star. The spherically symmetric structure of the atoms are destroyed and become cigar shape with the elongated axis along the direction of strong magnetic field. The atoms may even become almost an one dimensional string like object, i.e., needle shape, if the magnetic field strength is extremely high. In presence of ultra-strong magnetic field of strength $> 4.4 \times 10^{13}$G, the application of TF model for spherically symmetric WS cells is not a valid approximation [9]. However, one can use TF model for sylindrically deformed WS cells because of ultra-strong magnetic field [8,10,11,12]. In presence of ultra-strong magnetic field ($\gg 4.4 \times 10^{13}$G), the WS cells get magnetically deformed and become ellipsoidal in nature. In this article, for the sake of simplicity, we shall assume a cylindrical type deformation of the atoms in the inner crust region and use cylindrical coordinate system with azimuthal symmetry. In reality, to investigate the cigar like deformed atoms in presence of strong magnetic field one has to use prolate spheroidal coordinate system [13]. In future we shall present the problem related to structural deformation of atoms in a strong quantizing magnetic field using such coordinate system [13].

In the present article we shall study the properties of inner crust matter composed of magnetically deformed metallic atoms. In section 2 we have developed the basic formalism and discuss the numerical results, whereas in the last section we have given the conclusions and the future prospect of this work.

2 Basic formalism

The width of the outer crust of a typical neutron star is ~ 0.3 km, the density of matter, which is assumed to be a dense crystalline structure of metallic iron is $\sim 10^6 - 10^{11}$gm cm^{-3}, ranging from the upper edge to the bottom edge [14] respectively. In one of our previous work appeared i1n [6], the properties of outer crust region has been studied. To investigate the properties of such dense exotic crystalline matter of metallic iron, we have replaced the outer crust matter by a regular array of spherically symmetric WS cells, with positively charged nuclei at the centre surrounded by a non-uniform electron gas. Whereas in the inner crust region, of width $\sim 0.5 - 0.7$km and density $\sim 10^{11} - 10^{14}$gm cm^{-3}, we assume that since the magnetic field is high enough compared to outer crust region, the electron distribution around each nucleus (iron and also some neutron rich nuclei) gets deformed (the numerical values of widths and density ranges for various regions inside a neutron star strongly depends on the type of equation of state considered). They become cigar shape. In [7] we have studied the equation of states of inner crust matter with spherically symmetric electron distribution around each nucleus inside WS cells in presence of strong magnetic field. In this article for the sake of simplicity, we assume cylindrical type distribution of electron gas around each nucleus with the axis of each cylinder is along the direction of magnetic field and further assume azimuthal symmetry for all the cylindrically deformed WS cells. In this article, although we have considered magnetically deformed WS cells for electron distribution, the nuclei at the centre of these cells are assumed to be spherical in nature. We have also assumed that the magnetic field is not so strong to populate proton Landau levels and the magnetic (dipole) energy of neutron sector is negligibly small compared to the kinetic energy of these particles.

To investigate various physical properties of deformed electron distribution in the inner crust matter, we start with the Poisson's equation, given by

$$\nabla^2\phi = 4\pi e n_e \theta(\boldsymbol{r} - \boldsymbol{r_n}) - \frac{4\pi Ze}{V_n}\theta(\boldsymbol{r_n} - \boldsymbol{r}) \tag{1}$$

where $V_n = 4\pi r_n^3/3 = 4\pi r_0^3 A/3$, is the nuclear volume, $r_0 = 1.12$fm and A is the mass number of the nucleus [11, 12]. In the cylindrical coordonate system, if one assumes the magnetic deformation of atomic nuclei in this region, the θ-function associated with the contribution of protons within the nucleus has to be replaced by $\theta(\boldsymbol{r_n} - \boldsymbol{r})\theta(z_n - z)$, where in eqn.(1), Z is the atomic number of the nucleus, r_n is the nuclear radius, assumed to be spherical in shape, whereas in the above text, r_n and z_n given in the arguments of the θ-functions are respectively the radial and axial dimensions of the cylidrically deformed nucleus. However, in this article we have not assumed magnetic deformation of the nuclei. Here ϕ is the electrostatic field, e is the electron charge and n_e is the electron density, which because of assumed non-uniformity within the WS cells, is a function of positional coordinates (r, z). In our study, we shall consider the variation of $\phi(r, z)$ within the cylindrical distribution of the electrons surrounding the positively charged nucleus. Therefore, in the Poisson's equation the nuclear part as shown in eqn.(1) will not contribute. Now in the cylindrical coordinate with circular symmetry, the above equation reduces to

$$\frac{\partial^2\phi}{\partial r^2} + \frac{1}{r}\frac{\partial\phi}{\partial r} + \frac{\partial^2\phi}{\partial z^2} = 4\pi e n_e \tag{2}$$

It is well known that in presence of strong quantizing magnetic field, the number density of degenerate electron gas is given by

$$n_e = \frac{eB}{2\pi^2}\sum_{\nu=0}^{\nu_{max}}(2 - \delta_{\nu 0})p_F \tag{3}$$

where B is the constant external magnetic field, assumed to be acting along z-direction and is $> B_c^{(e)}$, where $B_c^{(e)}$ is the typical strength of magnetic field at and above which, in the relativistic scenario the Landau levels for the electrons are populated. For the sake of convenience, throughout this article we shall use natural units, i.e., $\hbar = c = 1$. The critical strength is then given by $B_c = m_e^2/\mid e \mid$ [6], where m_e is the electron rest mass and $\mid e \mid$ is the magnitude of electron charge. This critical strength may be obtained by equating the cyclotron quantum with the rest mass energy for electrons. We further assume that the matter is at zero temperature. In eqn.(3), p_F is the electron Fermi momentum, ν is the Landau quantum number, with ν_{max}, the upper limit of ν. The upper limit will be finite at zero temperature and infinity for finite temperature. The factor $(2 - \delta_{\nu 0})$ takes care of singly degenerate $\nu = 0$ state and doubly degenerate all other states with $\nu \neq 0$. To study the properties of inner crust matter with deformed WS cells, we make Thomas-Fermi approximation, which is semi-classical version of Hartree approximation [15]. In this model, the well known Thomas-Fermi condition is given by

$$\mu_e = (p_F^2 + m_e^2 + 2\nu eB)^{1/2} - e\phi = \text{constant} \tag{4}$$

where μ_e is the electron chemical potential, which is assumed to be constant throughout the WS cell. Hence one can express the Fermi momentum for electrons in the following form:

$$p_F = [(\mu_e + e\phi)^2 - m_e^2 - 2\nu eB]^{1/2} \tag{5}$$

Since the electrostatic potential $\phi \equiv \phi(r, z)$, the Fermi momentum p_F for the electron is also a function of positional coordinates (r, z) within the cell. In principle one should use this exact expression for electron Fermi momentum in the equation for electron density (eqn.(3)) which in turn appearing on the right hand side of the cylindrical form of Poisson's equation (eqn.(2)). However, with this exact expression for p_F, since the equation becomes non-linear in $\phi(r, z)$, it is absolutely impossible to proceed further analytically, even a single effective step. From the very beginning, therefore, one has to use some numerical technique to solve the Poisson's equation. Of course, with the numerical method within the limitation of the algorithm followed, more exact results can be obtained. However, in numerical computation of $\phi(r, z)$, we only get a set of numbers, but the beauty of this model will be completely destroyed and a lot of interesting physics associated with the intermediate results of this problem will be totally lost. Therefore, to get an approximate analytical solution for $\phi(r, z)$, as a first approximation, we set the upper limit for Landau quantum number $\nu_{max} = 0$ and also neglect the rest mass of electrons, i.e., we put $m_e = 0$ (since in the inner crust region the density of electron gas is high enough, the electron Fermi momentum will also be large compared to electron rest mass, therefore we expect that without appreciable error one can neglect electron mass in the above expression) in the expression for Fermi momentum p_F (eqn.(5)). The approximation $\nu_{max} = 0$ is actually valid if the magnetic field is extremely high ($\sim 10^{15}$G), perhaps is a valid approximation at the inner crust region for magnetars. However, to investigate some of the properties of dense electron gas within the cylindrically deformed WS cells to somewhat exact manner, later in this article, we shall use this approximate solution for $\phi(r, z)$ only, but do not use the first approximation $\nu_{max} = 0$ and $m_e = 0$ to evaluate mathematical expressions for various physical quantities of the dense electron gas. However. later in this article we shall show that the upper limit ν_{max} for the electron Landau quantum number is also a function of (r, z). Therefore to evaluate various physical quantities analytically in this region, first, one has to obtain an approximate solution for the Poisson's equation (with the values of $\nu_{max} = 0$ and $m_e = 0$ in the first approximation). To achieve our objectives, we use first the approximate form of electron Fermi momentum obtained from the assumption as mentioned above and its mathematical form is given by

$$p_F \approx \mu_e + e\phi \tag{6}$$

Next on substituting

$$\mu_e + e\phi(r, z) = \psi(r, z), \tag{7}$$

the cylindrical form of Poisson's equation reduces to

$$\frac{\partial^2\psi}{\partial r^2} + \frac{1}{r}\frac{\partial\psi}{\partial r} + \frac{\partial^2\psi}{\partial z^2} = \lambda^2\psi \tag{8}$$

where $\lambda^2 = 2e^3B/\pi$. From eqn.(8), it is quite obvious that under this approximation, the Poisson's equation reduces to a linear partial differential equation. To solve this equation analytically we use the method of separation of variables, given by

$$\psi(r, z) = R(r)L(z) \tag{9}$$

Substituting $\psi(r, z)$ from eqn.(9) in eqn.(8) and introducing a constant ξ, we get

$$\frac{d^2R}{dr^2} + \frac{1}{r}\frac{dR}{dr} + \xi^2 R = 0 \tag{10}$$

$$\frac{d^2L}{dz^2} - (\xi^2 + \lambda^2)L = 0 \tag{11}$$

where ξ is some real constant, independent of r and z but may change with the magnetic field strength and with the mass number and the atomic number of the type of elements present in this region. The solutions of eqns.(10) and (11) are well known. For eqn.(10), the solution is an ordinary Bessel function of order zero with the argument ξr, whereas for eqn.(11), it is an exponentially decaying function of z. In the language of mathematics, the solution for $\psi(r, z)$ is then given by

$$\psi(r, z) = CJ_0(\xi r)exp\left[\pm(\xi^2 + \lambda^2)^{1/2}z\right] \tag{12}$$

where + and − signs are for $z < 0$ or > 0 respectively. We consider a convenient form of cylindrical coordinate system, such that $z = 0$ plane is at the middle of the finite size cylinder. In that case we have to take positive sign for the upper half of the cylinder and negative sign for the lower half. Here C is a constant (again may change with the magnetic field strength and with the nuclear properties of the elements present in the inner crust region) and $J_0(\xi r)$

is the Bessel function of order zero. Now on the nuclear surface, at the centre of the WS cells, $\phi = Ze/r_n$ [16], where Z is the atomic number and $r_n = r_0 A^{1/3}$ is the nuclear radius, $r_0 = 1.12$fm and A is the mass number. We consider eqn.(12) at various point on the nuclear surface. To evaluate the parameters C and ξ numerically, we do the following: put $r = \alpha r_n$ and $z = \beta r_n$ at a particular point on the nuclear surface and also consider $r = \beta r_n$ and $z = \alpha r_n$ for another point, with $\alpha^2 + \beta^2 = 1$. Then we have

$$\psi(\alpha r_n, \beta r_n) = C J_0(\alpha r_n \xi) \exp\left[-(\xi^2 + \lambda^2)^{1/2} \beta r_n\right] = \mu_e + \frac{Ze^2}{r_n} \tag{13}$$

and

$$\psi(\beta r_n, \alpha r_n) = C J_0(\beta r_n \xi) \exp\left[-(\xi^2 + \lambda^2)^{1/2} \alpha r_n\right] = \mu_e + \frac{Ze^2}{r_n} \tag{14}$$

From eqn.(14) we have

$$C = \frac{1}{J_0(\beta r_n \xi) \exp\left[-(\xi^2 + \lambda^2)^{1/2} \alpha r_n\right]} \left[\mu_e + \frac{Ze^2}{r_n}\right] \tag{15}$$

Combining eqns.(13)-(14) we get

$$J_0(\alpha r_n \xi) \exp\left[-(\xi^2 + \lambda^2)^{1/2} \beta r_n\right] = J_0(\beta r_n \xi) \exp\left[-(\xi^2 + \lambda^2)^{1/2} \alpha r_n\right] \tag{16}$$

Hence we can write

$$\exp\left[-(\xi^2 + \lambda^2)^{1/2} r_n (\beta - \alpha)\right] = \frac{J_0(\beta r_n \xi)}{J_0(\alpha r_n \xi)} \tag{17}$$

This is a highly transcendental equation for ξ. However, it is possible to evaluate ξ numerically from this equation for a given magnetic field strength and for a given type of element, e.g., for metallic iron. To obtain ξ numerically we express eqn.(17) in the following convenient form

$$\xi^2 + \lambda^2 = \frac{1}{r_n^2 (\beta - \alpha)^2} \left[\ln\left\{\frac{J_0(\beta r_n \xi)}{J_0(\alpha r_n \xi)}\right\}\right]^2 \tag{18}$$

To evaluate numerical values for ξ, we now put (a) r and z values of the equator and poles of the nucleus, (b) $r = r_n/4$, (c) $r = r_n/2$ and (d) $r = 3r_n/4$, for four different positions on the nuclear surface and obtain four different sets of ξ as a function of magnetic field strength. For all these cases the z-coordinates are obtained from the relation $z = (r_n^2 - r^2)^{1/2}$. Because of the symmetry about $z = 0$ plane, the choice of negative values for α and β will give identical results. In fig.(1) we have plotted ξ (in MeV) as a function of magnetic field strength B, expressed in terms of critical magnetic field strength $B_c^{(e)}$, for the specific values of r and z as indicated above by (a), (b), (c) and (d). For all these cases, the variations are insensitive for the low and moderate values of magnetic field strengths. This figure shows that beyond field strength 10^{17}G, ξ increases sharply for all the cases. It is also obvious from fig.(1) that the parameter ξ not only varies with the strength of magnetic field but also more strongly depends on the positional coordinates on the nuclear surface, giving one of the boundary conditionss. In fig.(2) we have plotted the same kind of variations for the parameter C with the magnetic field strength, expressed in the same unit as in fig.(1) and also considering the same positions on the nuclear surface as considered for fig.(1). For low and moderate magnetic field values it is also almost constant, then it falls abruptly beyond 10^{17}G and finally saturates to some constant values. Since beyond 10^{17}G, electrons within the cells occupy their zeroth or very low lying Landau levels, the quantum mechanical effect of magnetic field becomes extremely important in this region and as a consequence both ξ and C change significantly beyond this magnetic field value. Since the magnetic field is not ultra strong to distort atomic nuclei, we have therefore considered spherical nuclei of radii $r_0 A^{1/3}$, at the z and r symmetric position inside the cylinder. From the solutions of eqns.(13) and (14), we have noticed that the functional form of the solution given by eqn.(12) does not change, but the unknown parameters C and ξ can have a large number of roots. As a result the final solution of Poisson's equation becomes degenerate (which has been shown in figs.(1) and (2)). As an hypothetical case, instead of spherically symmetric nuclei, we have replaced them by cylindrically deformed nuclei with axially symmetric nucleon distribution. The smaller cylinder (deformed nucleus) is coaxial with the bigger one and with identical $z = 0$ plane. For the surface potential we have used eqn.(52) of Appendix A. In eqn.(52) we have replaced r_{max} and z_{max} by r_n and z_n, the maximum values of r and z for the deformed nuclei. Here r_1 and z_1 are the surface values of r and z coordinates at any arbitrary point on the nuclear surface. To make the nucleon distributions within the nuclei axially symmetric, we put $\theta_1 = 0$. Of course, in such a geometrical configuration one of the geometrical parameter, e.g., either r_n or z_n has to be chosen arbitrarily, and the other one can be expressed in terms of the known one. Further, to choose one of the parameters, we assume that the nucleus is incompressible, as a consequence, the density will not change even if the geometrical configuration has changed. Then we have the simple relation $r_n^2 z_n = 3A/4r_0^3$. In this expression,

if we choose one of the unknown arbitrarily (with the numerical value very close to the nuclear radius), the other can also be known. However, we have noticed that in this case the degree of degeneracy is even more than the spherically symmetric case. Along the curved surface for the nuclei, for $r_1 = r_n$, we can have along the positive direction of z-axis, any value of z from 0 to z_n. Whereas on the plane faces, we have $z = z_n$ and r_1 can have any value from 0 to r_n. All these points are on the cylindrically deformed nuclear surface and the potential on the surface is given by eqn.(52). Hence we may conclude that a non-degenerate solution can only be obtained, if and only if the electron distribution is spherically symmetric and the nucleus is also spherical with a common centre (concentric spheres). Which we have studied previously [6]. However, we expect that if both the electron distribution and the shape of the nucleus at the centre are ellipsoidal in nature with the major axis (which is common for both the ellipsoids) along the magnetic field and two other axes (again common for both of them) are symmetric, the problem of degenerate solutions for electric potential inside WS cells will be removed. At present we are persuing this analysis. We believe that with this type of geometrical configuration, the electric field at the surface of the WS cell will also vanish, which is non-zero in the cylindrical case as discussed below..

Although the WS cells are overall charge neutral, at any point (r_{max}, z) on the curved surface and at any point (r, z_{max}) on the plane faces the potential $\psi(r, z)$ can not be a constant, here r_{max} and z_{max} are transverse and half longitudinal dimensions. Which further means that the electric field at the surface (both radial and longitudinal components) can not be zero. This is a purely geometrical effect and such a deformed charge distribution exhibit quadrupole moment. The modified form of electro-static potential at any point on the curved face of the cylindrically deformed WS cell is given by

$$\psi(s, \theta) = CJ_0(\xi r_{max}) \exp(-\Lambda s \sin\theta), \tag{19}$$

whereas on the plane faces, this potential is given by

$$\psi(s, \theta) = CJ_0(\xi s \cos\theta) \exp(-\Lambda s \sin\theta) \tag{20}$$

where $s = (r_{max}^2 + z^2)^{1/2}$ for the curved face and $= (r^2 + z_{max}^2)^{1/2}$ for the plane faces, and $\Lambda = (\lambda^2 + \xi^2)^{1/2}$ is a constant. Here the variable θ is introduced to obtain the variation of z on the curved surface and also r on the plane faces. Therefore this θ variable is not the conventional θ coordinate used in cylindrical system. From eqns.(18) and (19), it is obvious that the potential can not be constant on the surfaces. The corresponding electric field on the curved surface is given by

$$\boldsymbol{E} = \frac{\partial\psi}{\partial s}\hat{e_s} + \frac{1}{s}\frac{\partial\psi}{\partial\theta}\hat{e_\theta} \tag{21}$$

$$= -2C \exp(-\Lambda(s^2 - r_{max}^2)^{1/2})(J_0(\xi r_{max})\Lambda\hat{e_z} + J_1(\xi r_{max})\xi\hat{e_r}) \tag{22}$$

Similarly the electric field at the plane faces is given by

$$\boldsymbol{E} = \frac{\partial\psi}{\partial s}\hat{e_s} + \frac{1}{s}\frac{\partial\psi}{\partial\theta}\hat{e_\theta} \tag{23}$$

$$= -2C \exp(-\Lambda z_{max})(J_0(\xi(s^2 - z_{max}^2)^{1/2})\Lambda\hat{e_z} + J_1(\xi(s^2 - z_{max}^2)^{1/2})\xi\hat{e_r}) \tag{24}$$

Which are obviously non vanishing on the surface of WS cells. However, neighboring cylindrical WS cells will interact electro-magnetically because of the non-zero values of electrostatic fields at the surfaces. Due to some kind of electro-magnetic induction there will be charge polarization on the surfaces of cylindrically deformed WS cells. As a result a number of charged (induced by the nearest neighbor WS cells) WS cells will form a bundle of charge neutral WS cylinders, instead of a single cylindrical cell [17]. Again we expect that with ellipsoidal coordinate system, the non-zero electric field problem at the WS cell surface will also be solved.

Now from the Thomas-Fermi condition, we have

$$p_F = [\psi^2(r, z) - m_\nu^2]^{1/2} \tag{25}$$

where $m_\nu = (m_e^2 + 2\nu eB)^{1/2}$. With this exact expression for p_F, the number density for electron gas can be expressed as

$$n_e(r, z) = \frac{eB}{2\pi^2}\sum_{\nu=0}^{\nu_{max}}(2 - \delta_{\nu 0})[\psi^2(r, z) - m_\nu^2]^{1/2} \tag{26}$$

This is obviously more exact than eqn.(3), where the value of Fermi momentum p_F is taken from eqn.(6). Further, this expression shows that the electron density is a function of both r and z within the WS cells. Which actually justifies the assumption that the electron distribution inside each WS cell around the fixed nucleus is non-uniform. Now from the non-negative nature of p_F^2, we have

$$\nu_{max} = \frac{\psi^2(r, z) - m_e^2}{2eB} = \nu_{max}(r, z) \tag{27}$$

The upper limit of Landau quantum number ν_{max} will therefore also depend on the positional coordinates r and z within and on the curved surface and the plane faces of the cylinder. In our model, the upper limit of Landau quantum number is zero at the deformed WS cell surface. Had the electron distribution at the crustal region been homogeneous, like electron gas in a highly conducting metal, with a background of positively charged nuclei at rest, the value of ν_{max} would have remain same at all points and for all the electrons depending on the density of electron gas and the strength of magnetic field. However, in our model, the electrons are distributed in an axially symmetric cylinder around a symmetrically placed positively charged nuclei of spherical in shape. The electrostatic potential changes with r and z accordingly following eqns.(9) and (12). From the nature of such variation, we found that ν_{max} is maximum near the nuclear surface and vanishes at the WS surfaces (both curved surface and the plane faces). Therefore replacing both r and z by their maximum values r_{max} and z_{max} respectively, we have

$$\nu_{max}(r_{max}, z_{max}) = 0 \tag{28}$$

Further, from the overall charge neutrality of the WS cells we can write

$$Z = 2\pi e \int_{r_n}^{r_{max}} \int_{r_n}^{z_{max}} n_e(r,z) r dr dz = \quad \text{constant} \tag{29}$$

These two equations (eqns.(28) and (28)) are solved numerically to obtain r_{max} and z_{max} for various values of magnetic field strength for the inner crust matter with metallic iron only. Knowing both r_{max} and z_{max}, if we solve the equations $\nu_{max}(r, z_{max}) = 0$ and $\nu_{max}(r_{max}, z) = 0$ numerically for r (ranges from 0 to r_{max}) and z (ranges from 0 to z_{max}), which are on the surface of the cylinder, one can generate the whole surface of the cylinder, including the plane faces.

In fig.(3) we have plotted electron number density obtained from eqn.(26), in terms of normal nuclear density multiplied by 10^4, as a function of radial distance from nuclear surface to the WS cell boundary for the magnetic field strengths 10^1, 5×10^2, 5×10^3, 10^4 and 5×10^4 times $B_c^{(e)}$, indicated by the curves a, b, c, d and e respectively (In all the plots, we have used the values of C and ξ for the boundary condition on the equator and poles of the spherically symmetric nucleus. Although theoretically speaking the electrostatic potential inside the WS cells are degenerate with respect to the boundary condition on the nuclear surface, in practice, we have noticed from the numerical calculation that the variation with other points as the boundary is not so appreciable). These curves show that the electron number density is maximum near the nuclear surface and minimum near the WS cell boundary r_{max}. This figure also shows that electron number density increases with the strength of magnetic field. In fig.(4) we have plotted the same quantity as in fig.(3) but against the axial distance z from the nuclear surface to the WS cell boundary (plane faces) indicated by z_{max}. In this case also the variations are exactly same, qualitatively and quantitatively, as in fig.(3). The little qualitative difference is because of different types of functional dependencies. In fig.(5) we have plotted the upper limit of Landau quantum number ν_{max} as a function of radial coordinate from the nuclear surface to the WS cell boundary. In this figure the upper curve is for $10 \times B_c^{(e)}$, the middle one is for $10^2 \times B_c^{(e)}$ and the lower one is for $500 \times B_c^{(e)}$. The value of ν_{max} decreases with the increase in magnetic field strengths. It has been observed that beyond $500 \times B_c^{(e)}$, ν_{max} becomes identically zero throughout the WS cell. Further, the value of ν_{max} for $B \leq 500 \times B_c^{(e)}$ is largest near the nuclear surface and exactly zero near the cell boundary. In fig.(6) we have plotted the same kind of variation of ν_{max}, but against the axial distance from nuclear surface to the cell boundary. The qualitative and the quantitative variations are exactly identical with fig.(5). These two figures show that the electrons are completely spin polarized in the direction opposite to the external magnetic field $\boldsymbol{B}$ at the cell boundary, including the plane faces, even for $B \leq 500 \times B_c^{(e)}$, but beyond this value they are polarized at all the points within the cells. Although the variations along radial and axial directions are shown in these two figures, we expect that such polarized picture of electron gas exists throughout the cylindrically deformed WS cell surface, including the two plane faces. To explain the phenomenon of electron spin polarization within the WS cells, one has to solve Dirac equation in presence of strong magnetic field. It is then trivial to show that the Landau quantum number ν is given by: $2\nu = 2n + 1 + \alpha$, where $n = 0, 1, 2, ...$ is the principal quantum number and $\alpha = \pm 1$ are the eigen-values of spin operator σ_z corresponding to up and down spin states of electrons respectively. Hence it is quite obvious that all the Landau levels with $\nu \neq 0$ are doubly degenerate (with two possible combinations of n and α), whereas zeroth order Landau level is singly degenerate with only possible combination is $\nu = 0$ is $n = 0$ and $\alpha = -1$. Which actually mean that in the zeroth Landau level spins of all the electrons are aligned in the direction opposite to the external magnetic field. This is a kind of electron spin polarization under the influence of ultra-strong magnetic field, occurring at the surface region of WS cells, and also throughout the cells beyond some magnetic field strength. This type of spin polarization will not be observed if electrons satisfy schrödinger equation, even if we introduce electron spin by hand. Therefore, the spin polarization is a purely relativistic effect. In fig.(7) we have shown the variation of z_{max} with the strength of magnetic field B. This figure shows that the variation is almost insensitive for low and moderate magnetic field strengths but decreases almost abruptly beyond 10^{16}G, when most of the electrons occupy their zeroth Landau level, and finally tends to saturate to a constant value ~ 10fm. The variation of r_{max} with the strength of magnetic field is shown in fig.(8). The nature

of variation is more or less same as that of z_{max}. However, we have noticed that for extremely large field strength, $r_{max} \longrightarrow 0$, instead of saturation. This is a remarkable difference from its longitudinal counter part. It actually shows that in presence of extremely strong magnetic field the cylindrically deformed WS cells become more and more thin in the transverse direction. We therefore conclude that with the increase in magnetic field strength the radial contraction will be enormous compared to the axial one. From figs.(7)-(8) we have noticed that the variations are most significant beyond $B = 10^{16}$G. The reason is again because the electrons occupy only their zeroth Landau level in presence of such strong magnetic field, at which the quantum mechanical effect of the magnetic field dominates. In these two figures we have taken $Z = 26$ and $A = 56$, which are the atomic number and mass number respectively for the deformed iron atoms.

Next we calculate the different kinds of energies associated with the electron gas within WS cells. The cell averaged kinetic energy density of the electron gas is given by

$$\epsilon_k = \frac{2}{V}\frac{eB}{2\pi^2}\int d^3r \sum_{\nu=0}^{\nu_{max}}(2-\delta_{\nu 0}) \int_0^{p_F(r,z)} dp_z[(p_z^2+m_\nu^2)^{1/2}-m_e] \tag{30}$$

where in the cylindrical coordinate system with azimuthal symmetry $d^3r = 2\pi r dr dz$, with the limits $r_n \leq r \leq r_{max}$ and $r_n \leq z \leq z_{max}$ and $V = \pi r_{max}^2 2z_{max}$, the volume of each cell. The p_z integral is trivial, which gives an analytical expression for the local kinetic energy density i.e., at a particular point (r, z) within the WS cell. The factor 2 in the expression for V is for z-symmetry about $z = 0$ plane. In fig.(9) we have plotted the variation of local kinetic energy density as a function of radial distance r from the nuclear surface to the cell boundary for various magnetic field values, keeping $z = 0$. This figure shows that the kinetic energy density increases with the increase in magnetic field strength. We have indicated the curves by a, b, c, d and e for the magnetic field strengths $10B_c^{(e)}$, $5\times10^2B_c^{(e)}$, $5\times10^3B_c^{(e)}$, $10^4B_c^{(e)}$ and $5\times10^4B_c^{(e)}$ respectively. In fig.(10) we have shown the same kind of variations along axial distance from the nuclear surface to one of the plane faces of the WS cell. The variation with magnetic field strength is again almost identical with fig.(9). Similar to the variation of electron number density within the cell (fig.(3) and fig.(4)), both from fig.(9) and fig.(10) it may be concluded that the local kinetic energy density for electron gas is maximum near the nuclear surface and minimum at the cell boundary.

Similarly, the cell averaged electron-nucleus interaction energy per unit volume is given by

$$E_{en} = -\frac{2}{V}Ze^2\int d^3r\frac{n_e(r,z)}{(r^2+z^2)^{1/2}} \tag{31}$$

Analogous to the local kinetic energy density, here also one can obtain the local interaction energy per unit volume, $E_{en}(r, z)$ at a particular point within the cell. In fig.(11), the variation of the magnitude of electron-nucleus interaction energy per unit volume with the radial distance is plotted. In this figure we have indicated the curves by a, b, c, d and e for the magnetic field strengths $10B_c^{(e)}$, $5\times10^2B_c^{(e)}$, $5\times10^3B_c^{(e)}$, $10^4B_c^{(e)}$ and $5\times10^4B_c^{(e)}$ respectively. This figure shows that the magnitude of electron-nucleus local interaction energy increases with the increase in magnetic field strength. Which means that with the increase in magnetic field strength the electrons become more strongly bound by the Lorentz force of the form $e\boldsymbol{v}\times\boldsymbol{B}$. In fig.(12) we have shown the same kind of variation along z-axis. Both the qualitative and the quantitative nature of variations with the strength of magnetic field are same as that of fig.(11).

It is also obvious from figs.(9)-(12) that for a given magnetic field strength the kinetic energy density and the magnitude of electron-nucleus interaction energy per unit volume at a particular point, either along axial direction or in the radial direction, inside WS cells are of the same order of magnitude. We do expect that the same type of variations will be obtained at all the points inside the WS cells. In fig.(13) we have shown the variation of cell averaged kinetic energy of electron gas (solid curve) and the magnitude of cell averaged electron-nucleus interaction energy (dashed curve) with the magnetic field strength. This figure shows that both the quantities are increasing function of magnetic field strength. However, for low and moderate field values, the variations are not very much sensitive, particularly for the kinetic energy part of electron gas.

Next we consider the cell averaged electron-electron direct interaction energy density, given by

$$E_{ee}^{dir} = \frac{1}{V}e^2\int d^3r n_e(r,z)\int d^3r' n_e(r',z')\frac{1}{[(\boldsymbol{r}-\boldsymbol{r'})^2+(z-z')^2]^{1/2}} \tag{32}$$

Assuming $\boldsymbol{r}$ as the reference axis, we have $(\boldsymbol{r}-\boldsymbol{r'})^2 = r^2+r'^2-2rr'\cos\theta$, where θ is the angle between $\boldsymbol{r}$ and $\boldsymbol{r'}$, assumed to be on the same plane. Then $d^3r' = r'dr'd\theta dz'$, with $0 \leq \theta \leq 2\pi$. In this case the z integral has to be broken into two parts, one with limit $-z_{max} \leq z \leq \overline{z}$ and the other one with the limit $\overline{z} \leq z \leq +z_{max}$. The value of $\overline{z}$ is not easy to evaluate in the region between z-axis and r-axis. With θ symmetry, for the sake of simplicity we put

$\overline{z} = r_n$ and expect that the error will be nominal. Now to obtain electron-electron direct interaction energy one has to evaluate the five dimensional integral as shown in eqn.(32). None of them can be obtained analytically, hence it is necessary to follow some numerical methods. Even the θ integral can not be obtained analytically. One can express the θ integral in the form of an elliptical integral of first kind, given by

$$I_{\mathcal{EL}}(r, r', z, z') = \int_0^{\pi/2} d\theta \frac{1}{(1 - K\cos^2\theta)^{1/2}} \tag{33}$$

where $K = 4rr'/[(r + r')^2 + (z - z')^2]$. The direct part is then given by

$$E_{ee}^{dir} = \frac{4}{2V} e^2 \int d^3r n_e(r, z) \int r' dr' dz n_e(r', z') \frac{1}{[(r + r')^2 + (z - z')^2]^{1/2}} I_{\mathcal{EL}}(r, r', z, z') \tag{34}$$

where the factor 4 is coming from the angular integral over θ from 0 to 2π. Let us now consider the elliptic integral (eqn.(33)) on $z = 0$-plane. In this case both z and z' are zero and the factor $K = 1$. Then it can be shown very easily that the integral given by eqn.(33) will diverge at the lower limit. To avoid this unphysical infinity we put a lower cut-off (infrared cut-off) δ, which will now the lower limit for θ. The physical meaning of non-zero lower limit for the θ-integral is that the two electrons under consideration can not be at zero distance from each other on the arc of a circle whose centre is same as that of the nucleus. The infrared cut-off δ which is a measure of minimum angular distance between two neighboring electrons must necessarily depends on the minimum possible linear distance between them and also on the average radial distance from the centre of the nucleus. From a very elementary geometrical construction it can be shown that

$$\delta = \frac{s}{r} \tag{35}$$

where s is the arc length, or the distance between two neighboring electrons on the circular arc. Since s is infinitesimal in nature, we can approximate it by a straight line of length s, which is the length of the cord connecting two points occupied by two neighboring electrons. Since s is the minimum possible linear distance between two electrons, we can express it in terms of electron density near those points, given by

$$s \sim n_e^{-1/3} \tag{36}$$

The cell averaged electron-electron direct energy has been obtained by evaluating the multi-dimensional integrals numerically.

The electron-electron exchange energy corresponding to the ith electron in the cell is given by

$$E_{ee}^{(ex)} = -\frac{e^2}{2} \sum_j \int d^3r d^3r' \frac{1}{[(\boldsymbol{r} - \boldsymbol{r'})^2 + (z - z')^2]^{1/2}} \bar{\psi}_i(\boldsymbol{r}, z) \bar{\psi}_j(\boldsymbol{r'}, z') \psi_j(\boldsymbol{r}, z) \psi_i(\boldsymbol{r'}, z') \tag{37}$$

where $\psi_i(r, z)$ is the spinor wave function of Dirac equation in cylindrical coordinate in presence of strong quantizing magnetic field, and $\bar{\psi}(\boldsymbol{r}, z) = \psi^\dagger(\boldsymbol{r}, z)\gamma_0$, the adjoint of the spinor and γ_0 is the zeroth part of the Dirac gamma matrices γ_μ in cylindrical coordinate system. We have evaluated the cell averaged exchange energy using Dirac spinors in cylindrical coordinate. An elaborate discussion is given in the Appendix.

The kinetic pressure of non-uniform electron gas within the WS cell is given by

$$P(r, z) = \frac{eB}{2\pi^2} \sum_{\nu=0}^{\nu_{max}(r,z)} (2 - \delta_{\nu 0}) \int_0^{p_F(r,z)} \frac{p_z^2 dp_z}{(p_z^2 + m_\nu^2)^{1/2}} \tag{38}$$

The p_z integral is very easy to evaluate analytically and is given by

$$P(r, z) = \frac{eB}{4\pi^2} \sum_{\nu=0}^{\nu_{max}(r.z)} \Big[p_F (p_F^2 + m_\nu^2)^{1/2} - m_\nu^2 \ln \left\{ \frac{p_F + (p_F^2 + m\nu^2)^{1/2}}{m_\nu} \right\} \Big] \tag{39}$$

which gives the local pressure at (r, z). This equation shows that the electron kinetic pressure also changes from point to point within the WS cells. In fig.(14) we have shown the variation of kinetic pressure for the non-uniform electron gas with the radial distance within the cell. Curves a and b are for $B = 10 \times B_c^{(e)}$ and $B = 500 \times B_c^{(e)}$, whereas upper curve and lower curve as indicated by c (almost identical) are for $B = 5000 \times B_c^{(e)}$ and $B = 10000 \times B_c^{(e)}$ respectively.

In fig.(15) the same kind of variations are shown along z-axis. In this figure the curves for $B = 5000 \times B_c^{(e)}$ and $B = 10000 \times B_c^{(e)}$ are almost identical and indicated by single thick curve c. For $B = 10 \times B_c^{(e)}$ and $B = 500 \times B_c^{(e)}$ the curves are indicated by a and b respectively. These two figures show that the kinetic pressure is maximum near the nuclear surface and zero at the cell boundary. The variation with magnetic field strength shows that the non-uniform electron gas becomes softer for higher magnetic field within the cells. In fig.(16) we have shown the variation of cell averaged electron-electron direct interaction energy (solid curve) and the corresponding kinetic pressure (dashed curve) with the magnetic field strength. Both the quantities are monotonically increasing function of magnetic field strength. Since in TOV equation for neutron stars, in the equation of state the cell averaged electron gas kinetic pressure is used, hence we can conclude that since electron gas becomes harder in presence of strong magnetic field in this particular region, the width of inner crust region will increase with the increase in magnetic field strength. In fig.(17) we have shown the variation of cell averaged electron-electron exchange interaction energy, assuming the extreme case when electrons occupy only their zeroth Landau level (dashed curve) and the most general one, when electrons can have all possible Landau levels (solid curve). The figure shows that for $\nu \neq 0$, the exchange energy is oscillatory for low and moderate values of magnetic field strength. This oscillatory phenomenon is identical with the observed De Haas-van Alphen oscillation observed in Landau diamagnetism. The exchange energy becomes extremely small when the electron Fermi momentum suddenly becomes zero for some value of magnetic field strength and then rises sharply upto a certain magnitude of magnetic field strength and finally decreases to zero, when the magnetic energy dominates over the matter part. In the case of $\nu = 0$, the nature of variation is almost identical, except the oscillatory nature at low and moderate magnetic field region.

For the sake of completeness, we have obtained the classical form of electron-electron Coulomb potential energy and the corresponding electron-nucleus interaction energy within a WS cell. The electron-electron interaction energy is given by (an elaborate discussion is given in the Appendix)

$$E_{ee} = \frac{Z^2e^2}{r_{max}^4 z_{max}^2} \int_0^\infty \frac{dk}{k^5} [r_{max} J_1(kr_{max}) - r_n J_1(kr_n)]^2 \\ [k(z_{max} - r_n) - (1 - \exp\{-k(z_{max} - r_n)\})] \tag{40}$$

and the corresponding electron-nucleus interaction part is given by

$$E_{en} = -\frac{Z^2e^2}{r_{max}^2 z_{max}} I \tag{41}$$

where

$$\begin{aligned} I = & \frac{1}{2}\left[(z_{max}^2 + r_{max}^2)^{1/2} z_{max} + r_{max}^2 \log\left(\frac{(z_{max}^2 + r_{max}^2)^{1/2} + z_{max}}{r_{max}}\right)\right] \\ & - \frac{1}{2}\left[(r_n^2 + r_{max}^2)^{1/2} r_n + r_{max}^2 \log\left(\frac{(r_n^2 + r_{max}^2)^{1/2} + r_n}{r_{max}}\right)\right] \\ & - \frac{1}{2}\left[(z_{max}^2 + r_n^2)^{1/2} z_{max} + r_n^2 \log\left(\frac{(z_{max}^2 + r_n^2)^{1/2} + z_{max}}{r_n}\right)\right] \\ & + \frac{1}{2}[2^{1/2} r_n^2 + r_n^2 \log(2^{1/2} + 1)] \end{aligned} \tag{42}$$

The detail derivations for electron-nucleus Coulomb interaction energy is also given in the Appendix. In fig.(18) we have shown the variation of electron-electron Coulomb energy density (solid curve) and the corresponding magnitude of electron-nucleus classical interaction energy density (dashed curve) with the strength of magnetic field. Both the curves show that the classical interaction energies are also insensitive to the strength of magnetic field in the low and moderate regions, and both of them are affected significantly beyond 10^{16}G. The reason is again that the electrons occupy only their zero-th Landau level. However, unlike the quantum mechanical cases, here at high magnetic field region both of them become extremely small. Moreover the overall magnitude does not change by an order of magnitude within the range of magnetic field considered. Finally to show that the cylindrically deformed WS cell structure of the inner crust matter of strongly magnetized neutron star (magnetar) is energetically favorable over the spherical structure, in fig.(19) we have compared the energy per electron for these two possible type of WS cell structures for various values of magnetic field strength. In this figure solid curve indicated by sph is for spherical cell structure and the dashed one indicated by cyl is for the cylindrically deformed WS cells. The energy per electron plotted along left y-axis is for the spherical case whereas for the cylindrical case the same quantity is plotted along right y-axis. This figure shows that for cylindrical case the total energy per electron is about one order of magnitude less than that of spherical case. Further beyond $B \sim 10^{17}$G, energy per electron for the cylindrical case becomes several orders of magnitude less than the spherical case (see also [19]).

3 Conclusions

In this article we have investigated various physical properties of non-uniform electron gas assuming cylindrically deformed atoms of metals, in particular the metallic iron at the inner crust of a strongly magnetized neutron star. Because of extremely strong surface magnetic field of magnetars, we have assumed a cylindrical type deformation of the atoms, which are subsequently replaced by WS cells with the same kind of geometrical structure. The longitudinal axis of all the cylinders are along the direction of magnetic lines of forces. The curved surfaces of these cylinders are therefore parallel to the boundary surface of the neutron stars in the region far away from the magnetic poles, where the magnetic lines of forces emerge almost perpendicularly with the surface (polar cap). We have studied various physical quantities for the dense electron gas in the inner crust region. We have investigated the variations with magnetic field strength for cell averaged quantities and also the spatial variations for constant magnetic field. We have noticed that the transverse dimension of a cylindrically deformed WS cell becomes extremely thin in presence of ultra-strong magnetic field. In this work we have also compared the total energy per electron with the spherical case and found that the cylindrically deformed WS structure in the inner crust region is energetically more favorable over the spherical case in presence of ultra-strong magnetic field. Although we have considered cylindrical type deformation for the iron atoms in this region, it is expected that the atoms become cigar shape in presence of strong magnetic field. The present investigation, assuming cylindrically deformed atoms is therefore an approximate model calculation. In our future study, the properties of neutron star inner crust matter with cigar shape atoms in the metallic crystal in presence of strong magnetic field will be investigated.

4 Appendix

A. Coulomb energy of electron gas:

1. Electron-nucleus Coulomb interaction energy:

$$E_{en} = -Ze\int_v \frac{dq}{s} \tag{43}$$

Where the integral is over the whole volume and $s = (r^2 + z^2)^{1/2}$. The charge element within an elementary volume dv is given by

$$dq = Ze\frac{dv}{v} = Ze\frac{rdrdz}{2r_{max}^2 z_{max}} \tag{44}$$

Hence

$$E_{en} = -\frac{Z^2e^2}{2r_{max}^2 z_{max}}\int_{r_n}^{r_{max}} rdr\int_{r_n}^{z_{max}} \frac{1}{(r^2+z^2)^{1/2}} \tag{45}$$

The double integral can very easily be evaluated and finally we get eqn.(40) as given in the text.

2. Electron-electron Coulomb interaction energy:

$$E_{ee} = \frac{1}{2}\int\int \frac{dq_1 dq_2}{s} \tag{46}$$

Where $s = [(z_1 - z_2)^2 + (\boldsymbol{r}_1 - \boldsymbol{r}_2)^2]^{1/2}$. In this case the charge elements dq_1 and dq_2 are at (r_1, θ_1, z_1) and (r_2, θ_2, z_2) respectively. The factor $1/2$ is to take care of double counting. From a very simple geometrical construction it can very easily be shown that

$$s = \left[(z_1 - z_2)^2 + (r_1^2 + r_2^2 - 2r_1r_2\cos(\theta_1 - \theta_2))\right]^{1/2} \tag{47}$$

Substituting for dq_1 and dq_2, with the definition as given in eqn.(42), we have

$$E_{ee} = \frac{1}{2}\frac{Z^2e^2}{4\pi^2 r_{max}^4 z_{max}^2}\int_{r_n}^{r_{max}} r_1dr_1\int_{r_n}^{r_{max}} r_2dr_2\int_{r_n}^{z_{max}} dz_1\int_{r_n}^{z_{max}} dz_2\int_0^{2\pi} d\theta_1\int_0^{2\pi} d\theta_2 \frac{1}{\left[(z_1 - z_2)^2 + (r_1^2 + r_2^2 - 2r_1r_2\cos(\theta_1 - \theta_2))\right]^{1/2}} \tag{48}$$

To evaluate the integrals, we use the identity

$$\frac{1}{s} = \frac{1}{\left[(z_1 - z_2)^2 + (r_1^2 + r_2^2 - 2r_1r_2\cos(\theta_1 - \theta_2))\right]^{1/2}} = \frac{1}{\pi}\sum_{m=-\infty}^{+\infty}\exp\{im(\theta_1 - \theta_2)\}\int_0^{\infty} J_m(kr_1)J_m(kr_2)\exp\{-k(z_> - z_<)\}dk \tag{49}$$

To obtain electron-electron Coulomb energy, we first evaluate the potential at (r_1, θ_1, z_1) due to a charge element $dq(r_2, \theta_2, z_2)$. This is given by

$$\phi(r_1, \theta_1, z_1) = \int \frac{dq(r_2, \theta_2, z_2)}{s} \tag{50}$$

Using the identity as defined above (eqn.(48)) and integrating over z_2, within the range $r_n \leq z_2 \leq z_{max}$, we get

$$\begin{aligned}\phi(r_1, \theta_1, z_1) = \frac{Ze}{2\pi r_{max}^2 z_{max}} \sum_{m=-\infty}^{+\infty} \int_0^{+\infty} \frac{dk}{k} \int_{r_n}^{r_{max}} r_2 dr_2 \int_0^{2\pi} d\theta_2 J_m(kr_1) J_m(kr_2) \\ (2 - \exp\{-k(z_1 - r_n)\} - \exp\{-k(z_{max} - z_1)\}) \exp\{im(\theta_1 - \theta_2)\}\end{aligned} \tag{51}$$

Integral over θ_2 gives $2\pi\delta_{m0}$, which means only $m = 0$ term of the series in the above identity (eqn.(48)). Hence, we have

$$\begin{aligned}\phi(r_1, \theta_1, z_1) = \frac{Ze}{r_{max}^2 z_{max}} \int_0^{\infty} \frac{dk}{k} \int_{r_n}^{r_{max}} r_2 dr_2 J_0(kr_1) J_0(kr_2) \\ (2 - \exp\{-k(z_1 - r_n)\} - \exp\{-k(z_{max} - z_1)\})\end{aligned} \tag{52}$$

Further, to evaluate the r_2 integral within the range $r_n \leq r_2 \leq r_{max}$, we use the relation

$$\int_0^x r dr J_m(r) = \frac{x\Gamma(\frac{m+2}{2})}{\Gamma(m/2)} \sum_{l=0}^{\infty} \frac{(\mid m \mid +2l+1)\Gamma(\frac{m}{2} + l)}{\Gamma(\frac{m+4}{2} + l)} J_{|m|+2l+1}(x) \tag{53}$$

Since $m = 0$, we have in the denominator of the above expression $\Gamma(m/2) = \infty$. Whereas the numerator of the first term of l series in the above relation (i.e., for $l = 0$ term) also contains a $\Gamma(m/2) = \infty$ term. These two terms will cancel each other and we get non-zero contribution for $l = 0$ only with $m = 0$. To evaluate r_2 integral we decompose it in the following form as given below

$$\int_{r_n}^{r_{max}} .....dr_2 = \int_0^{r_{max}} .....dr_2 - \int_0^{r_n} .....dr_2 \tag{54}$$

Then using eqn.(52) with $l = 0$ and $m = 0$, it is possible to evaluate r_2 integral analytically. Then we have the Coulomb potential due to the charge element $dq(r_2, \theta_2, z_2)$

$$\begin{aligned}\phi(r_1, z_1) = \frac{Ze}{r_{max}^2 z_{max}} \int_0^{\infty} \frac{dk}{k^2} \left[r_{max} J_1(kr_{max}) - r_n J_1(kr_n)\right] \\ J_0(kr_1) \left[2 - \exp\{-k(z - r_n)\} - \exp\{-k(z_{max} - z_1)\}\right]\end{aligned} \tag{55}$$

Hence it is also possible to evaluate the components of electric field, $E_z = -\partial\phi/\partial z_1$ along z-direction and $E_r = -\partial\phi/\partial r_1$ along the radial direction. It is trivial to show that these components are non-zero on the WS cell surface, including the plane faces. The Coulomb energy is then given by

$$E_{ee} = \frac{1}{2} \frac{Ze}{2\pi r_{max}^2 z_{max}} \int \phi(r_1, z_1, \theta_1) dq(r_1, z_1, \theta_1) \tag{56}$$

The θ_1 integral will give 2π, the z_1 integral is very easy to evaluate and for r_1 integral we use the Bessel integral formula as given in eqn.(52). Then we have the electron-electron Coulomb interaction energy

$$E_{ee} = \frac{Z^2 e^2}{r_{max}^4 z_{max}^2} \int_0^{\infty} \frac{dk}{k^5} \left[r_{max} J_1(kr_{max}) - r_n J_1(kr_n)\right]^2 \left[k(z_{max} - r_n) - (1 - \exp\{-k(z_{max} - r_n)\})\right] \tag{57}$$

B. Electron-electron exchange energy:

In the cylindrical coordinate system with the external magnetic field along z-axis, which is also the symmetry axis of the cylinder and considering the gauge $\boldsymbol{A}(\boldsymbol{r}) \equiv B(-y/2, x/2, 0)$, we have the Dirac equation corresponding to upper component $\phi_\lambda(\boldsymbol{r})$:

$$\left[E^2 - m^2 + 2\lambda k + \frac{\partial^2}{\partial\rho^2} + \frac{1}{\rho}\frac{\partial}{\partial\rho} + \frac{\partial^2}{\partial z^2} - k^2\rho^2\right] \phi_\lambda(\boldsymbol{r}) = 0 \tag{58}$$

where $k = eB/2$ and $\sigma_z \phi(\boldsymbol{r}) = \lambda\phi$ with $\lambda = \pm 1$, eigen-values for spin-up and spin-down states respectively. Defining $\beta_\lambda = E^2 - m^2 + 2\lambda k$, the above equation can be written in the following form.

$$\left[\beta_\lambda + \frac{\partial^2}{\partial\rho^2} + \frac{1}{\rho}\frac{\partial}{\partial\rho} + \frac{\partial^2}{\partial z^2} - k^2\rho^2\right] \phi_\lambda(\rho, z) = 0 \tag{59}$$

writing the solution for the upper component in the separable form: $\phi_\lambda(\rho,z) = f_\lambda(\rho)\exp(ip_z z)$, we have from the above equation

$$\left[\beta_\lambda + \frac{\partial^2}{\partial\rho^2} + \frac{1}{\rho}\frac{\partial}{\partial\rho} - k^2\rho^2\right] f_\lambda(\rho) = 0 \tag{60}$$

where β_λ is replaced by $\beta_\lambda - p_z^2$. The solutions are given by

$$f_\lambda(\rho) = \exp\left(-\frac{t}{2}\right) g_\lambda(t) \tag{61}$$

where $t = \eta^2 = k\rho^2$. Substituting $f_\lambda(\rho)$, we have

$$g_\lambda = \frac{N}{L}^{1/2} \exp(ip_z z)\exp\left(-\frac{t}{2}\right) L_n(t) \tag{62}$$

where L is the linear dimension along z-axis, $L_n(t)$ is the well known Laguerre polynomial,

$$\mid N \mid = \left[\frac{k}{2E}\left(1+\frac{m}{E}\right)\right]^{1/2} \tag{63}$$

is the normalization constant. Considering the effect of spin into account, we have

$$g_{\lambda=+1} = L_n\left(\frac{1}{2}eB\rho^2\right)\begin{pmatrix}1\\0\end{pmatrix} \tag{64}$$

and

$$g_{\lambda=-1} = L_n\left(\frac{1}{2}eB\rho^2\right)\begin{pmatrix}0\\1\end{pmatrix} \tag{65}$$

are the up-spin and down-spin states respectively for the upper component, with the corresponding energy eigen-values $E_+ = (p_z^2 + m^2 + 2neB)^{1/2}$ and $E_+ = (p_z^2 + m^2 + 2(n+1)eB)^{1/2}$.

The spin-up and spin-down spinor states are then given by

$$\psi^\uparrow(\rho,z) = \left[\frac{k}{2E}\left(1+\frac{m}{E}\right)\right]^{1/2} \frac{\exp(ip_z z)\exp\left(-\frac{t}{2}\right)}{L^{1/2}} \begin{pmatrix} L_n \\ 0 \\ p_z L_n/(E+m) \\ -2ik^{1/2}t^{1/2}/(E+m)L_n' \end{pmatrix} \tag{66}$$

and

$$\psi^\downarrow(\rho,z) = \left[\frac{k}{2E}\left(1+\frac{m}{E}\right)\right]^{1/2} \frac{\exp(ip_z z)\exp\left(-\frac{t}{2}\right)}{L^{1/2}} \begin{pmatrix} 0 \\ L_n \\ -2ik^{1/2}t^{1/2}/(E+m)(L_n' - L_n) \\ -p_z L_n/(E+m) \end{pmatrix} \tag{67}$$

Substituting for up-spin state, we have

$$\begin{aligned}\overline{\psi}_i^\uparrow(\boldsymbol{r})\psi_i^\uparrow(\boldsymbol{r}') = {} & \frac{k}{2\pi L}\left(1+\frac{m}{E}\right)\exp\{-ip_z(z-z') - \frac{1}{2}(t+t')\} \\ & \left\{\left(1 - \frac{p_z^2}{(E+m)^2}\right) L_n(t)L_n(t') - \frac{4k(tt')^{1/2}}{(E+m)^2} L_n'(t)L_n'(t')\right\}\end{aligned} \tag{68}$$

Similarly,

$$\begin{aligned}\overline{\psi}_i^\downarrow(\boldsymbol{r}')\psi_i^\downarrow(\boldsymbol{r}) = {} & \frac{k}{2\pi L}\left(1+\frac{m}{E}\right)\exp\left\{-ip_z(z-z') - \frac{1}{2}(t+t')\right\} \\ & \left[\left(1 - \frac{p_z^2}{(E+m)^2}\right) L_n(t)L_n(t') - \frac{4k(tt')^{1/2}}{(E+m)^2}\left\{(L_n'(t') - L_n(t'))(L_n'(t) - L_n(t))\right\}\right]\end{aligned} \tag{69}$$

Identical expressions can also be obtained for jth type particles, on which there is a sum. To obtain the exchange energy, we replace the sum over j by the integral over momentum p_z of jth particle, i.e., $\sum_j \to L\int dp_z'$. Assuming $\boldsymbol{r}$

as the reference axis, we can write $\int d^3x d^3x' ... = 2\pi \int \rho d\rho dz \rho' d\rho' dz' d\theta' ....$ Replacing the variables $z\prime$ and p'_z by two new variables, $\overline{z}$ and P_z, where $\overline{z} = z' - z$ and $P_z = p_z - p'_z$, we have the $\overline{z}$ integral

$$I = \int_{-\infty}^{+\infty} \frac{\exp(i\overline{z}P_z)}{(\overline{z}^2 + X^2)^{1/2}} d\overline{z} = 2K_0(XP_z) \tag{70}$$

where $X = \mid \boldsymbol{\rho} - \boldsymbol{\rho}' \mid$ and

$$K_0(x) = \int_0^{\infty} \frac{\cos(xt)}{(t^2+1)^{1/2}} dt \tag{71}$$

is the modified Bessel function of order zero. The z-integral simply gives L. The integral over P'_z can be obtained analytically using the following integrals (eqns.(71)-(72)):

$$I = \int_0^{2p_F} K_0(P_z \mid X \mid) dP_z = \frac{1}{\mid X \mid} \int_0^{\alpha} K_0(w) dw \tag{72}$$

where $\alpha = 2p_F \mid X \mid$ and p_F is the electron Fermi momentum. The value of the integral on the right hand side of the above equation is obtained from standard mathematical hand book [18] and is given by

$$\begin{aligned} \int_0^x K_0(t)dt = &-(\gamma + \log x/2)\ x \sum_{k=0}^{\infty} \frac{(x/2)^{2k}}{(k!)^2(2k+1)} \\ &+ x \sum_{k=0}^{\infty} \frac{(x/2)^{2k}}{(k!)^2(2k+1)^2} + x \sum_{k=1}^{\infty} \frac{(x/2)^{2k}}{(k!)^2(2k+1)} \times \\ &(1 + 1/2 + ... + 1/k) = xI(x) \end{aligned} \tag{73}$$

where γ (Euler's constant) $= 0.5772156649$. The rest three integrals, over ρ, ρ' and θ are evaluated numerically. The Laguerre polynomials $L_n(x)$ and their derivatives $L'_n(x)$ are obtained numerically from the recursion relations and derivative formulas from the reference as cited above and finally obtained the exchange energy as a function of magnetic field strength as defined in eqn.(36).

References

1. R.C. Duncan and C. Thompson, Astrophys. J. Lett. **392**, L9 (1992); C. Thompson and R.C. Duncan, Astrophys. J. **408**, 194 (1993); C. Thompson and R.C. Duncan, MNRAS **275**, 255 (1995); C. Thompson and R.C. Duncan, Astrophys. J. **473**, 322 (1996).
2. P.M. Woods et. al., Astrophys. J. Lett. **519**, L139 (1999); C. Kouveliotou, et. al., Nature **391**, 235 (1999).
3. K. Hurley, et. al., Astrophys. Jour. **442**, L111 (1999).
4. S. Mereghetti and L. Stella, Astrophys. Jour. **442**, L17 (1999); J. van Paradihs, R.E. Taam and E.P.J. van den Heuvel, Astron. Astrophys. **299**, L41 (1995); S. Mereghetti, astro-ph/99111252; see also A. Reisenegger, astro-ph/01003010; see also S. Mereghetti, arXiv:0904.4880v1, for current status on the observational aspects of magnetars.
5. see the review work by P.Haensel, A.Y.Potekhin and D.G.Yakovlev,Neutron Stars 1: Equation of State and Structure, Springer, Vol. 326 (2007).
6. Nandini Nag, Sutapa Ghosh and Somenath Chakrabarty, Ann. of Phys., **324**, 499 (2009).
7. Nandini Nag, Sutapa Ghosh and Somenath Chakrabarty, Euro. Phys. Jour. **A 45**, 99 (2010).
8. Jon Eilif Skjervold and Erlend Ostgaard, Phys. Scr., **29**, 484 (1984).
9. D. Lai, Rev. Mod. phys. **73**, 629 (2001).
10. B. K. Shivamoggi and P. Mulser, EPL, **22**, 657 (1993).
11. M. Rotondo, R. Ruffini and S. -S. Xue, arXiv:0903.4095.
12. M. Rotondo, J. A. Rueda, R. Ruffini and S. -S. Xue, arXiv:0911.4622.
13. Arpita Ghosh and Somenath Chakrabarty (in preparation).
14. S.L. Shapiro and S.A. Teukolsky, Black Holes, White Dwarfs and Neutron Stars, John Wiley and Sons, New York, (1983).
15. E.H. Lieb and B. Simon, Phys. Rev. Lett. **31**, 681 (1973); E.H. Lieb, J.P. Solovej and J. Yngvason, Phys. Rev. Lett. **69**, 749 (1992); E.H. Lieb, Bull. Amer. Math. Soc., **22**, 1 (1990);
16. R. Ruffini, "Exploring the Universe", a Festschrift in honour of Riccardo Giacconi, Advance Series in Astrophysics and Cosmology, World Scientific, Eds. H. Gursky, R. Rufini and L. Stella, vol. **13**, 383 (2000); Int. Jour. of Mod. Phys. **5**, 507 (1996).
17. M. Ruderman, Phys. Rev. Lett. **27**, 1306 (1971).
18. Hand Book of Mathematical Functions, Ed. M. Abramowitz and I.A. Stegun, Dover publication, INC., New York, 1970.
19. R. O. Mueller, A. R. P. Rau and Larry Spruch, Phys. Rev. Lett. **26**, 1136 (1971).

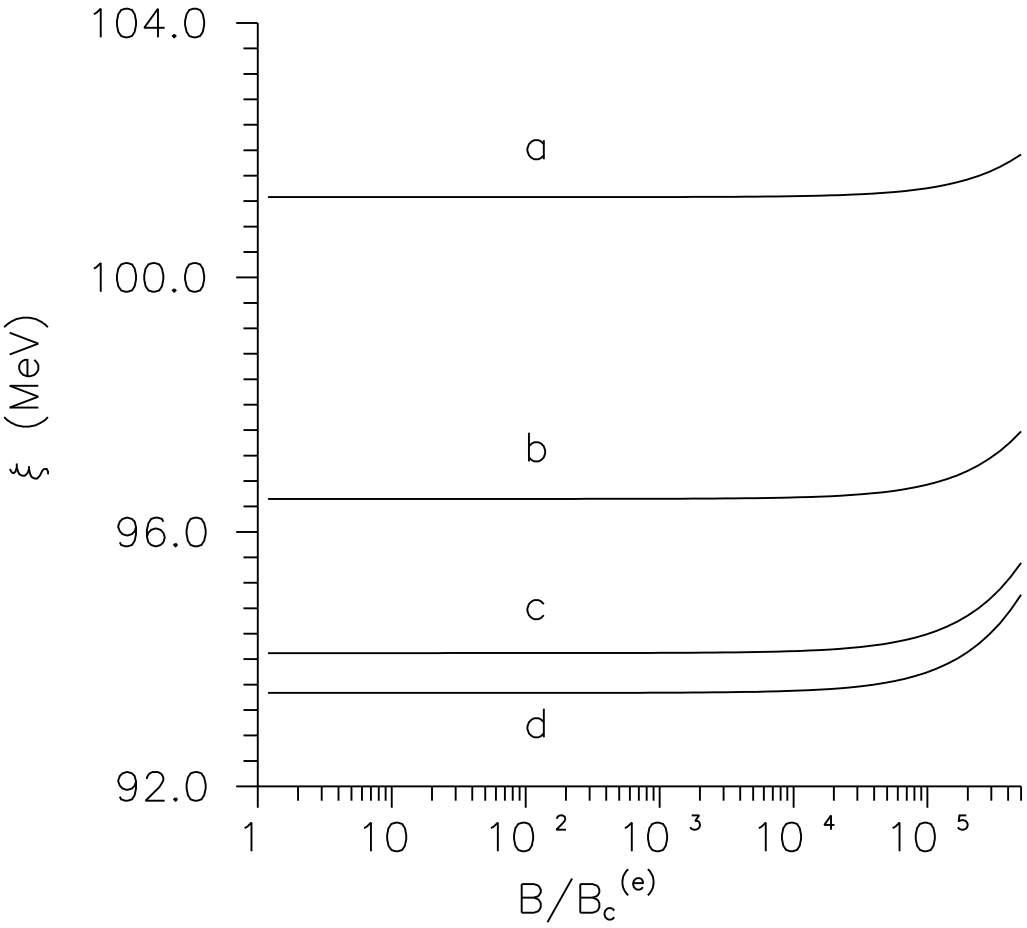

Fig. 1. The variation of separation variable ξ with the magnetic field strength. Curve (a): r and z are on the equator and poles respectively, curve (b): $r = r_n/4$, curve (c): $r = r_n/2$ and curve (d): $r = 3r_n/4$. For the curves (b),(c) and (d), $z = (r_n^2 - r^2)^{1/2}$.

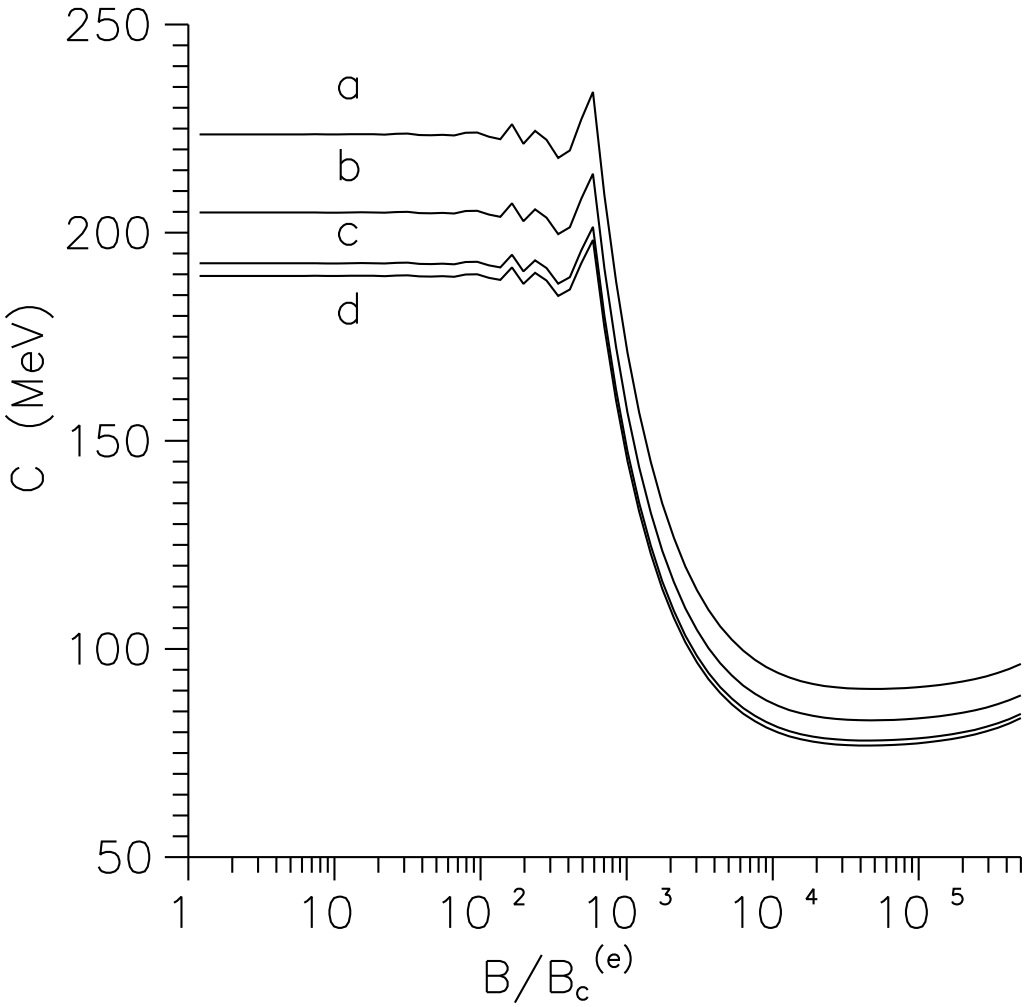

Fig. 2. The variation of normalization constant C with the magnetic field strength. Curve (a): r and z are on the equator and poles respectively, curve (b): $r = r_n/4$, curve (c): $r = r_n/2$ and curve (d): $r = 3r_n/4$. For the curves (b),(c) and (d), $z = (r_n^2 - r^2)^{1/2}$.

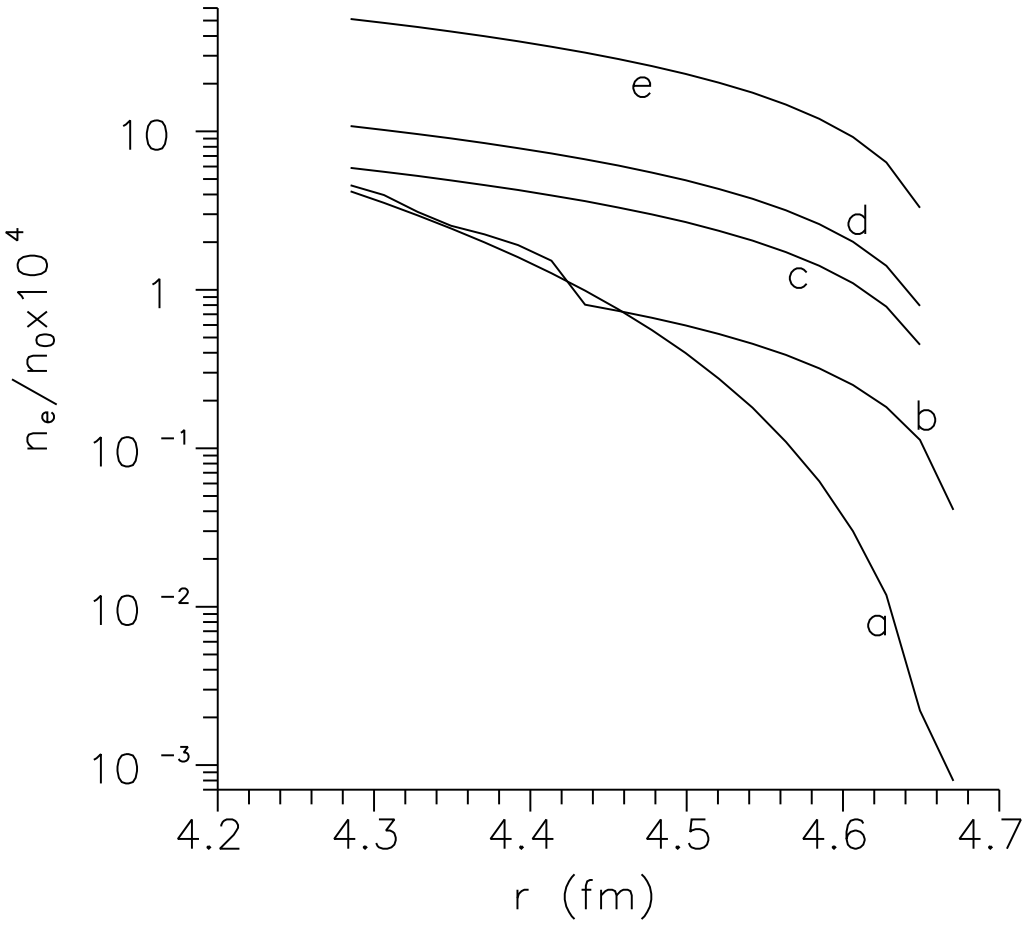

Fig. 3. The variation of electron number density expressed in terms of normal nuclear density with radial distance r in Fermi. The curves indicated by a, b, c, d and e are for $B = 10, 5 \times 10^2, 5 \times 10^3, 1 \times 10^4$ and 5×10^4 times $B_c^{(e)}$ respectively.

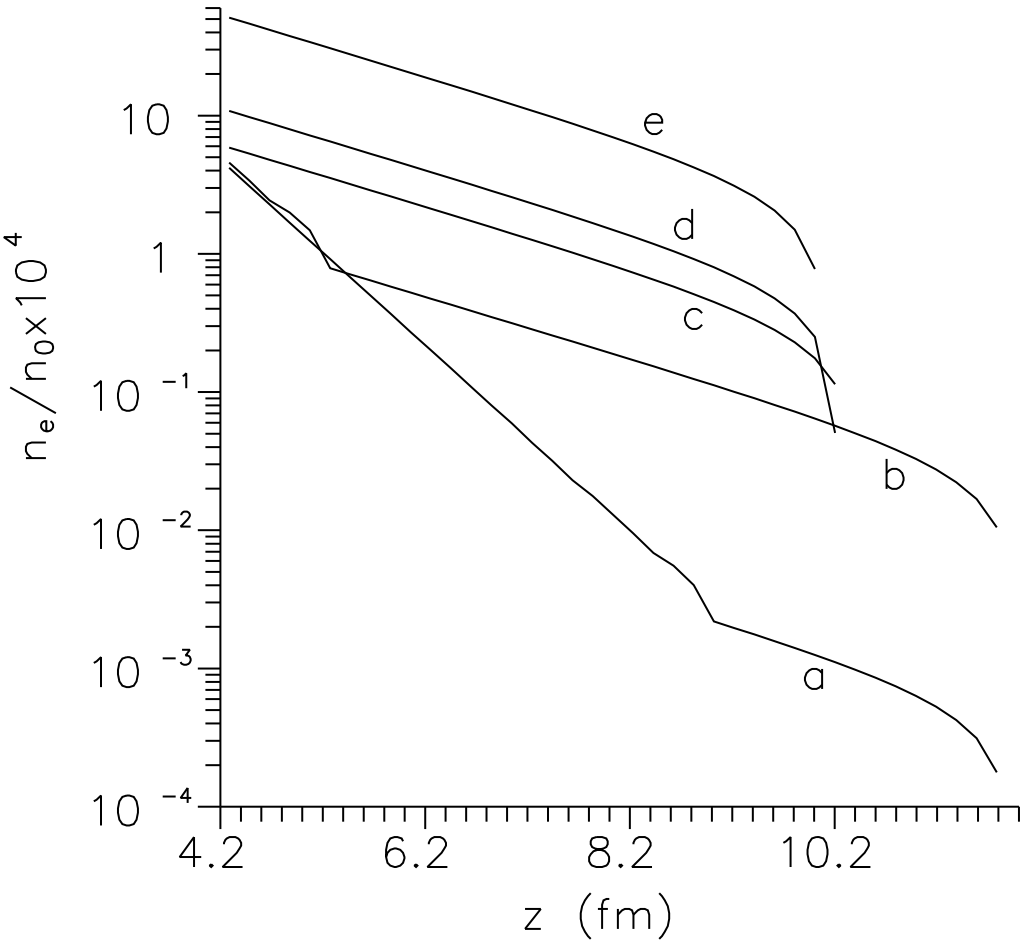

Fig. 4. The variation of electron number density expressed in terms of normal nuclear density with radial distance z in Fermi. The curves indicated by a, b, c, d and e are for $B = 10, 5 \times 10^2, 5 \times 10^3, 1 \times 10^4$ and 5×10^4 times $B_c^{(e)}$ respectively.

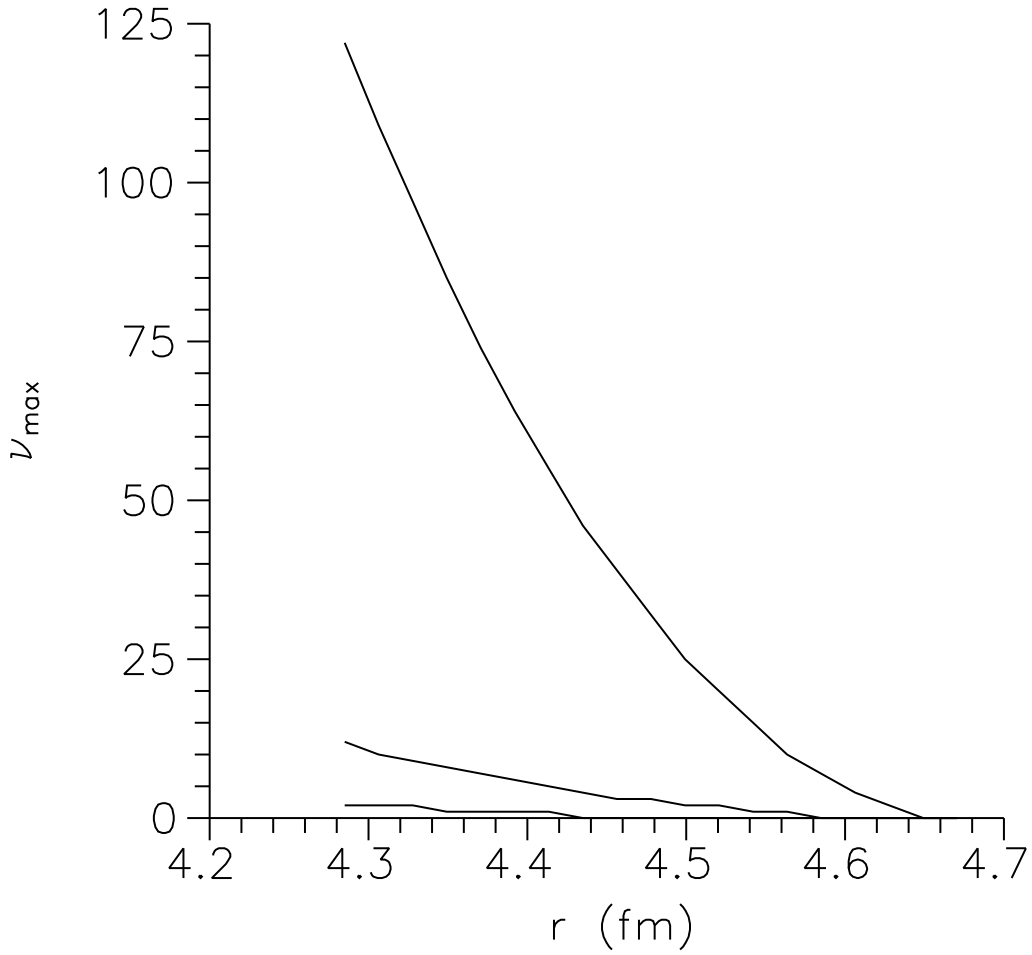

Fig. 5. The variation of upper limit of Landau quantum number with the radial distance in Fermi. Upper curve is for $B = 10 \times B_c^{(e)}$, middle one is for $10^2 \times B_c^{(e)}$ and the lower one is for $5 \times 10^2 B_c^{(e)}$.

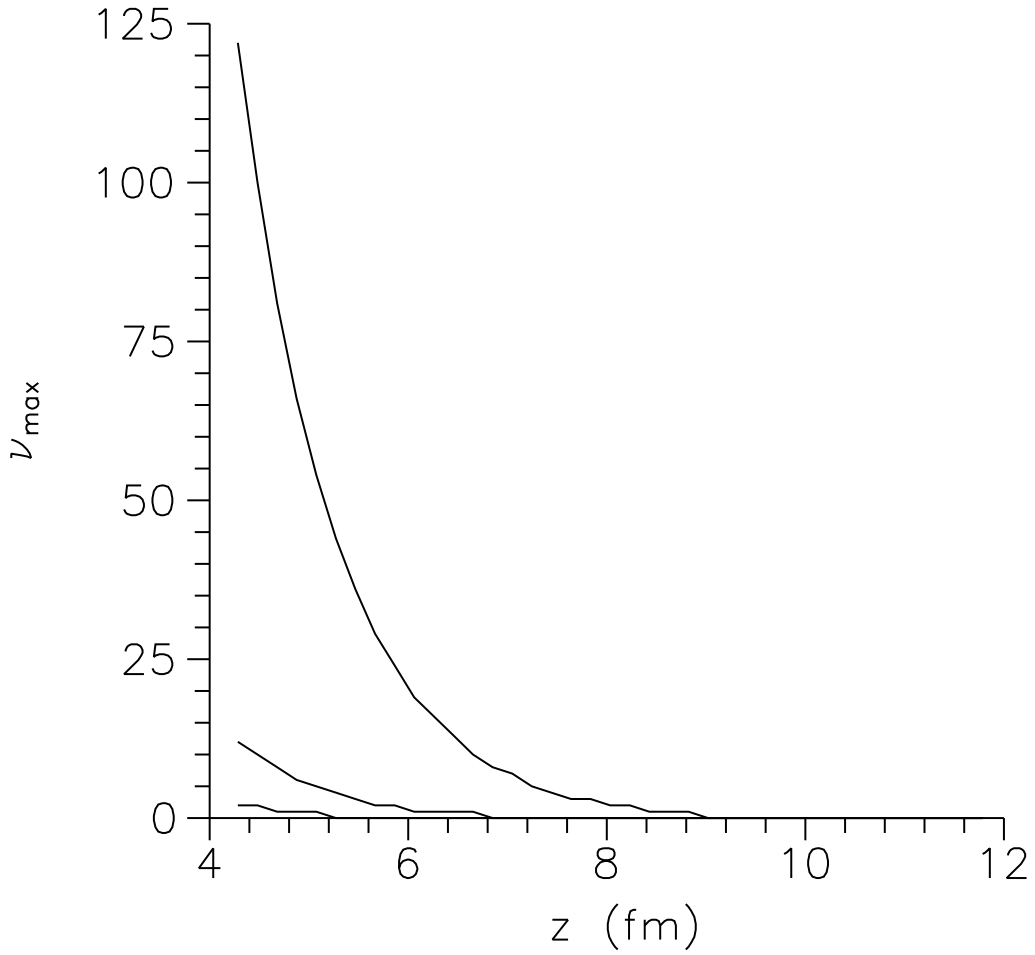

Fig. 6. The variation of upper limit of Landau quantum number with the axial coordinate. Upper curve is for $B = 10 \times B_c^{(e)}$, middle one is for $10^2 \times B_c^{(e)}$ and the lower one is for $5 \times 10^2 B_c^{(e)}$.

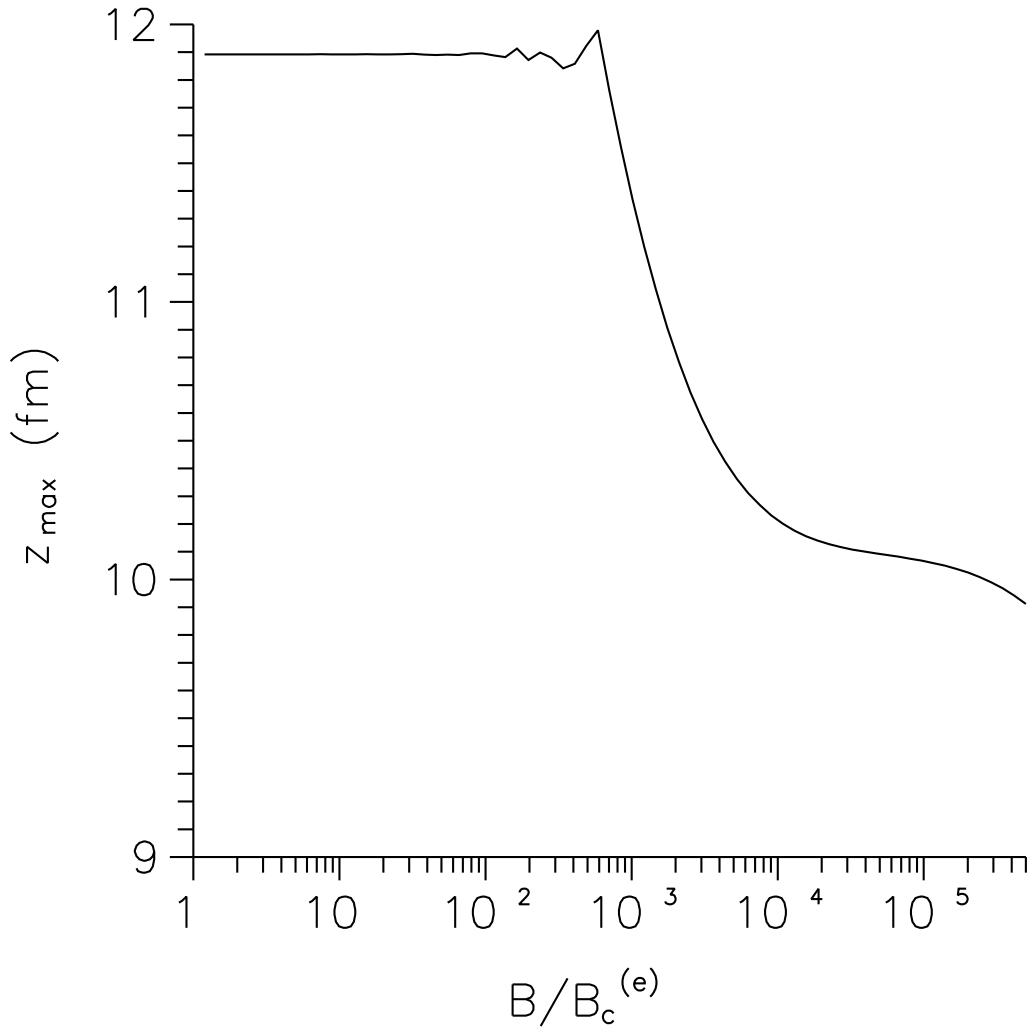

Fig. 7. The variation of z_{max} with the magnetic field strength.

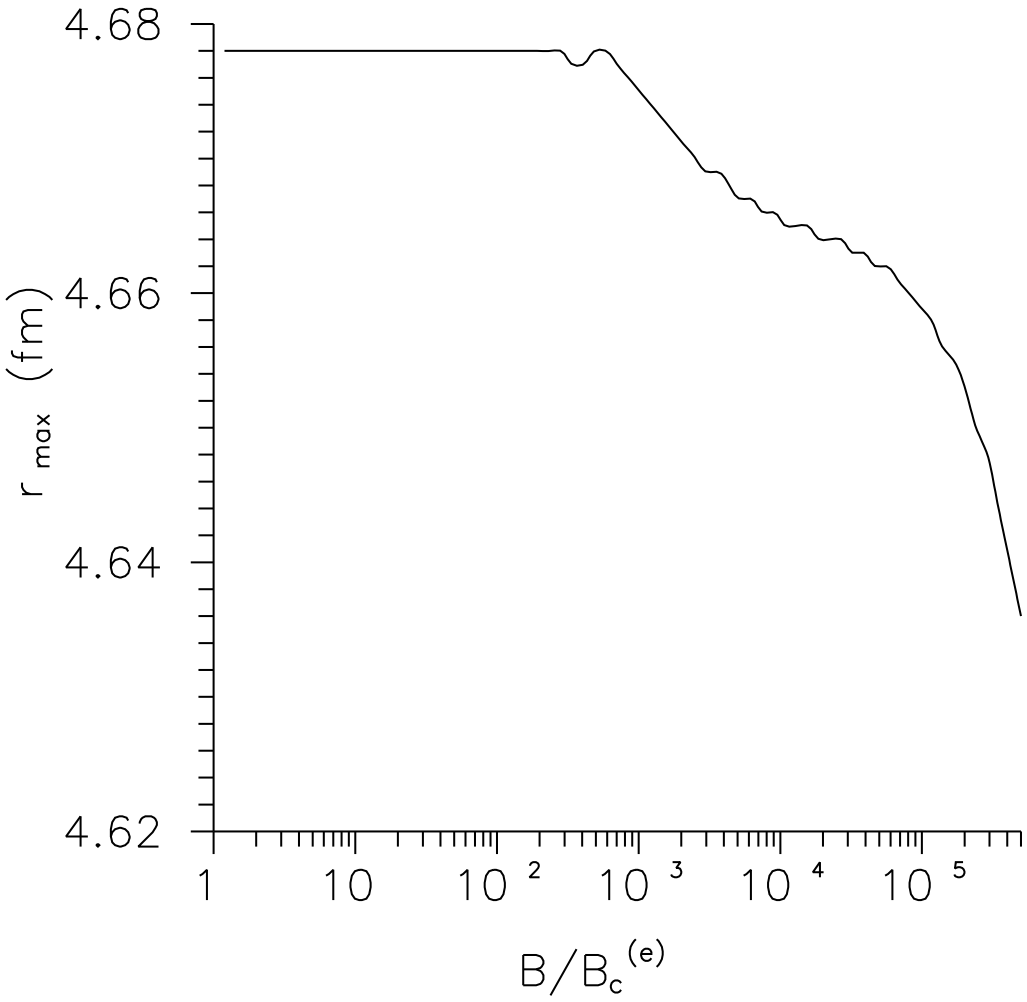

Fig. 8. The variation of r_{max} with the magnetic field strength.

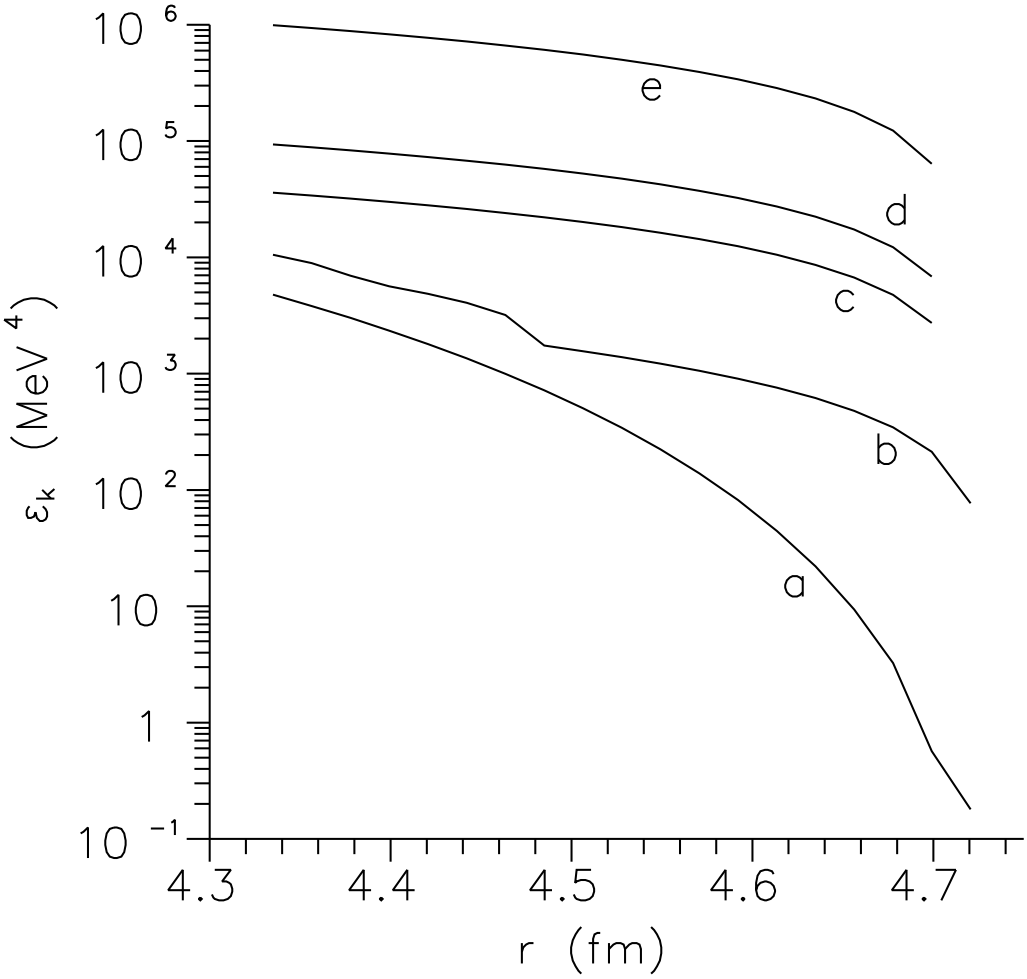

Fig. 9. The variation of kinetic energy density with the radial distance in Fermi. The curves indicated by a, b, c, d and e are for $B = 10, 5 \times 10^2, 5 \times 10^3, 1 \times 10^4$ and 5×10^4 times $B_c^{(e)}$ respectively.

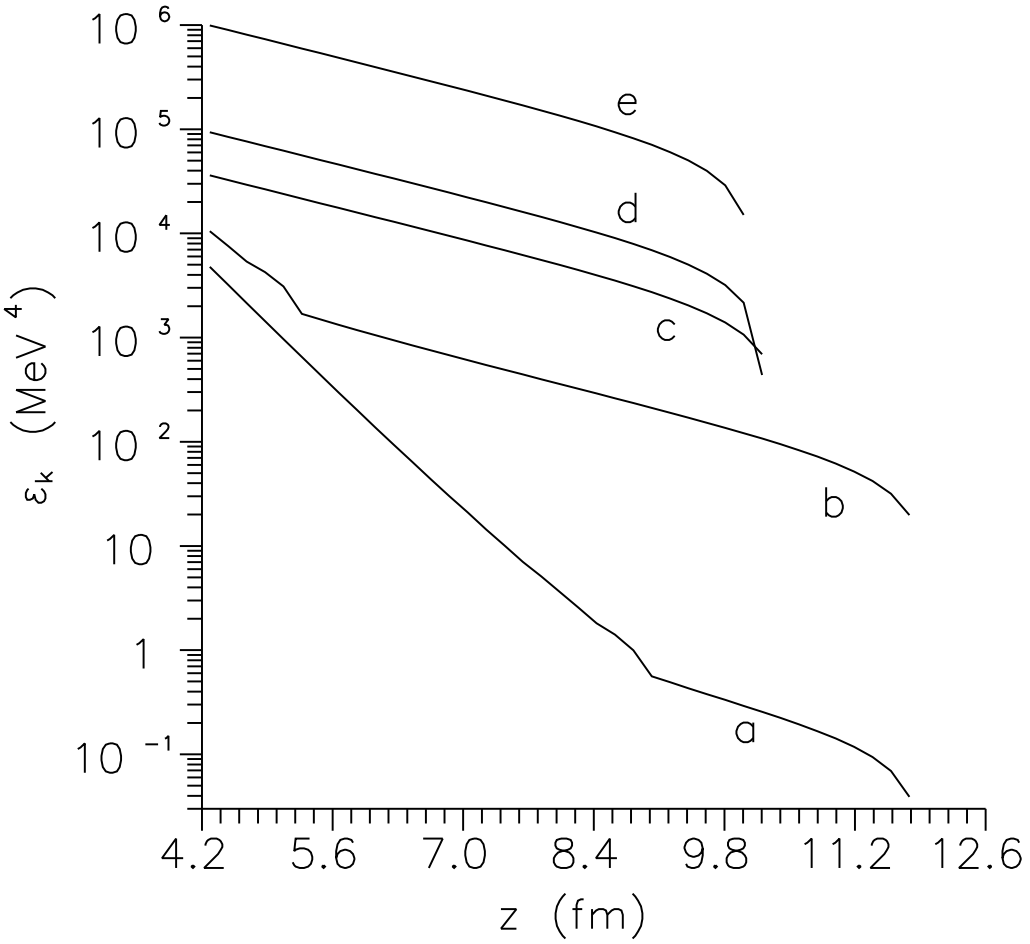

Fig. 10. The variation of kinetic energy density with the axial coordinate in Fermi. The curves indicated by a, b, c, d and e are for $B = 10, 5 \times 10^2, 5 \times 10^3, 1 \times 10^4$ and 5×10^4 times $B_c^{(e)}$ respectively.

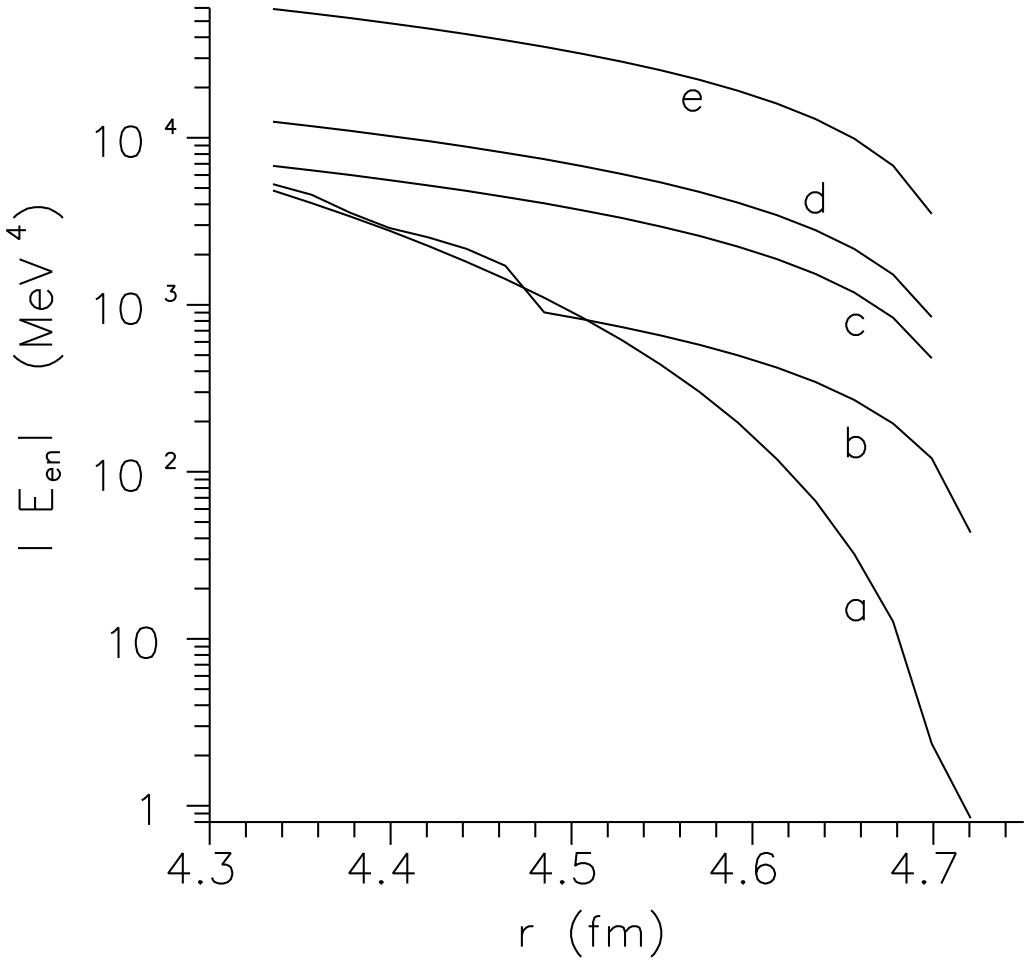

Fig. 11. The variation of the magnitude of electron nucleus interaction energy density with the radial distance in Fermi. The curves indicated by a, b, c, d and e are for $B = 10, 5 \times 10^2, 5 \times 10^3, 1 \times 10^4$ and 5×10^4 times $B_c^{(e)}$ respectively.

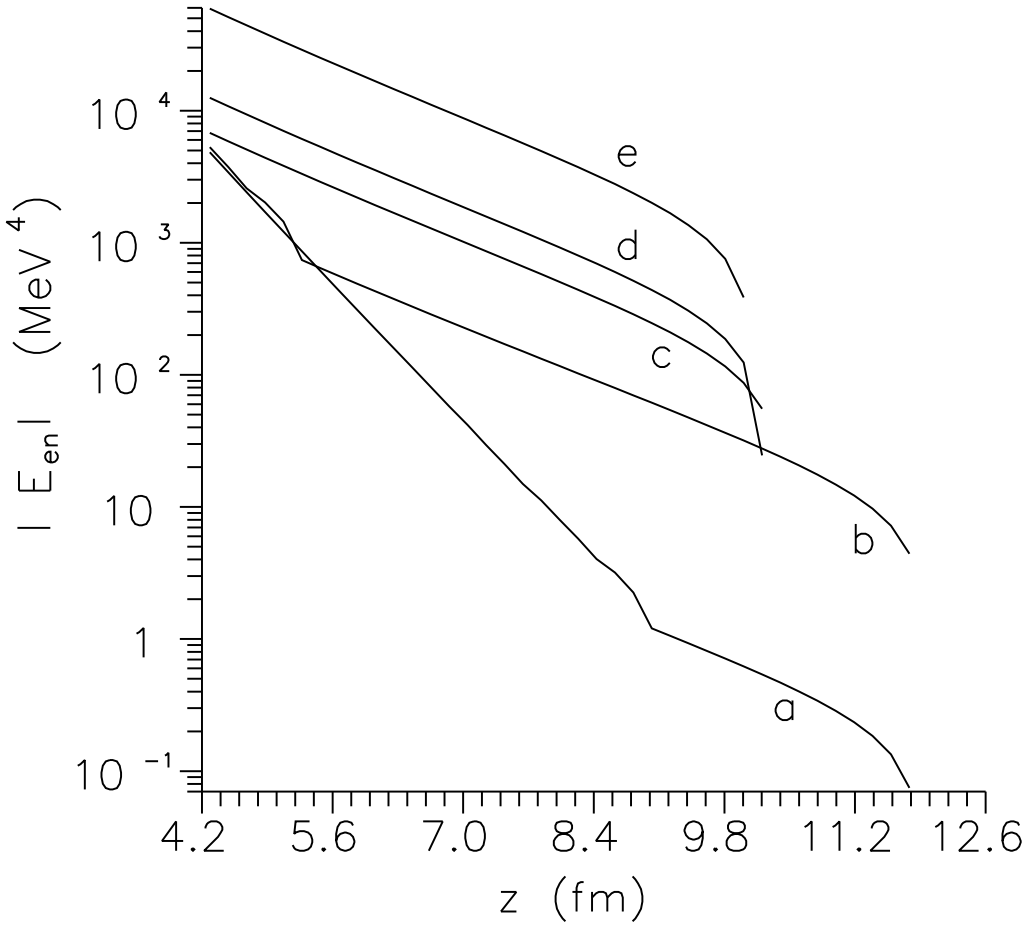

Fig. 12. The variation of the magnitude of electron nucleus interaction energy density with the axial coordinate in Fermi. The curves indicated by a, b, c, d and e are for $B = 10, 5 \times 10^2, 5 \times 10^3, 1 \times 10^4$ and 5×10^4 times $B_c^{(e)}$ respectively.

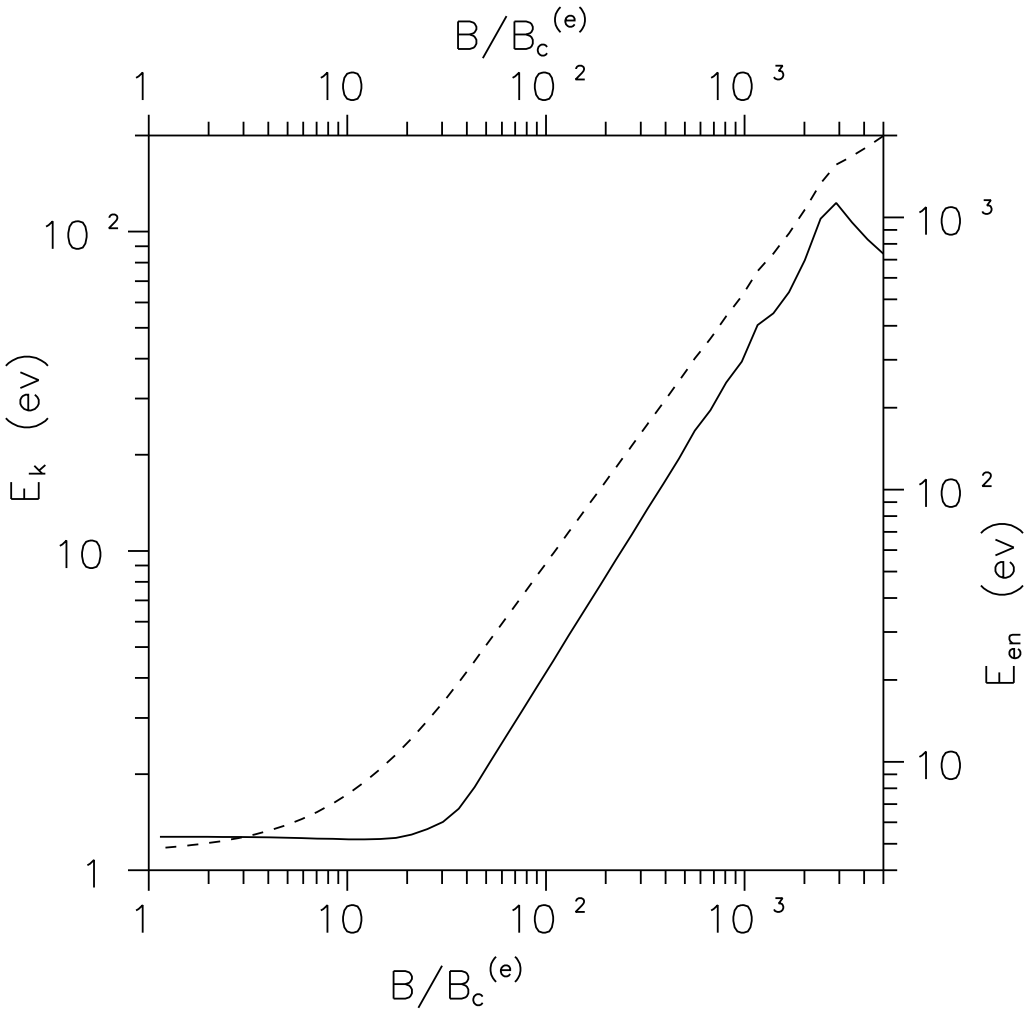

Fig. 13. The variation of cell averaged kinetic energy (solid curve) and cell averaged magnitude of the electron-nucleus interaction energy (dashed curve) with the strength of magnetic field.

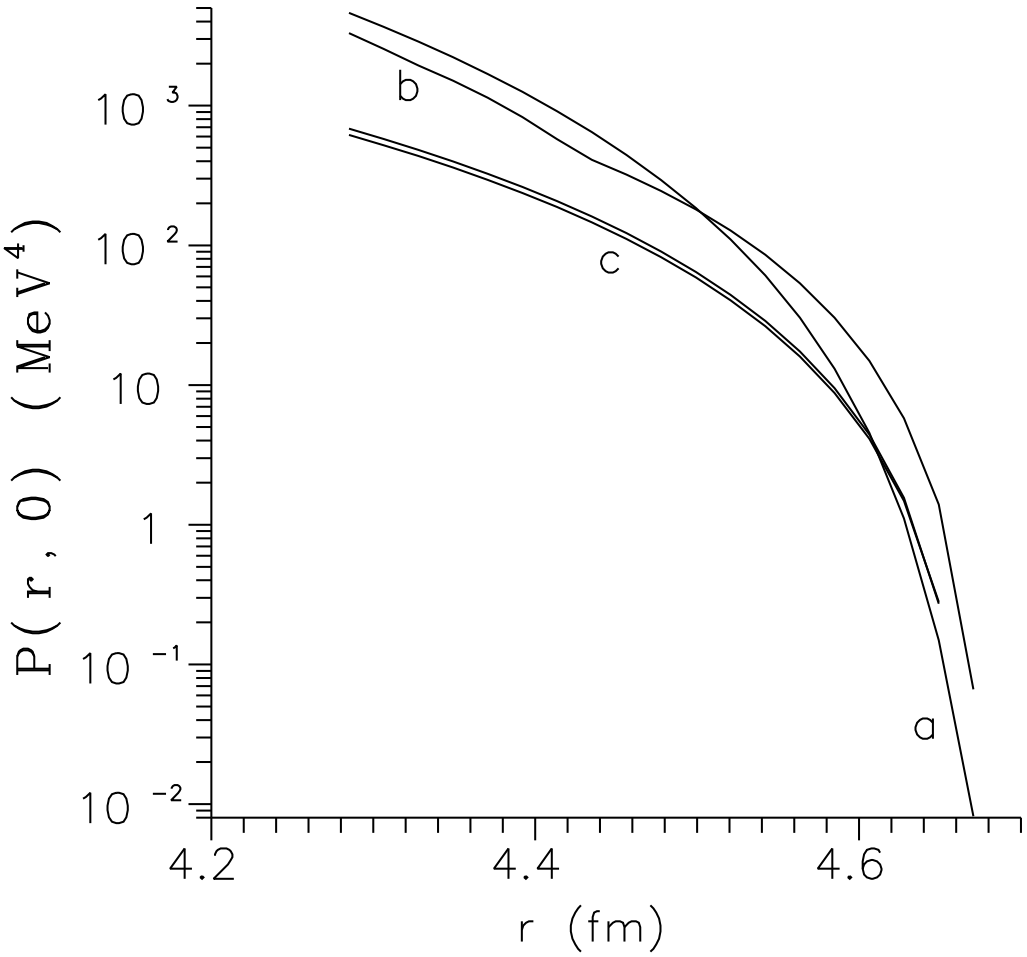

Fig. 14. The variation of kinetic pressure of non-uniform electron gas within WS cell with the radial distance in Fermi. Curves a and b are for $B = 10 \times B_c^{(e)}$ and $5 \times 10^2 B_c^{(e)}$ respectively, whereas upper and the lower curves indicated by c are for $5 \times 10^3 B_c^{(e)}$ and $10^4 \times B_c^{(e)}$ respectively.

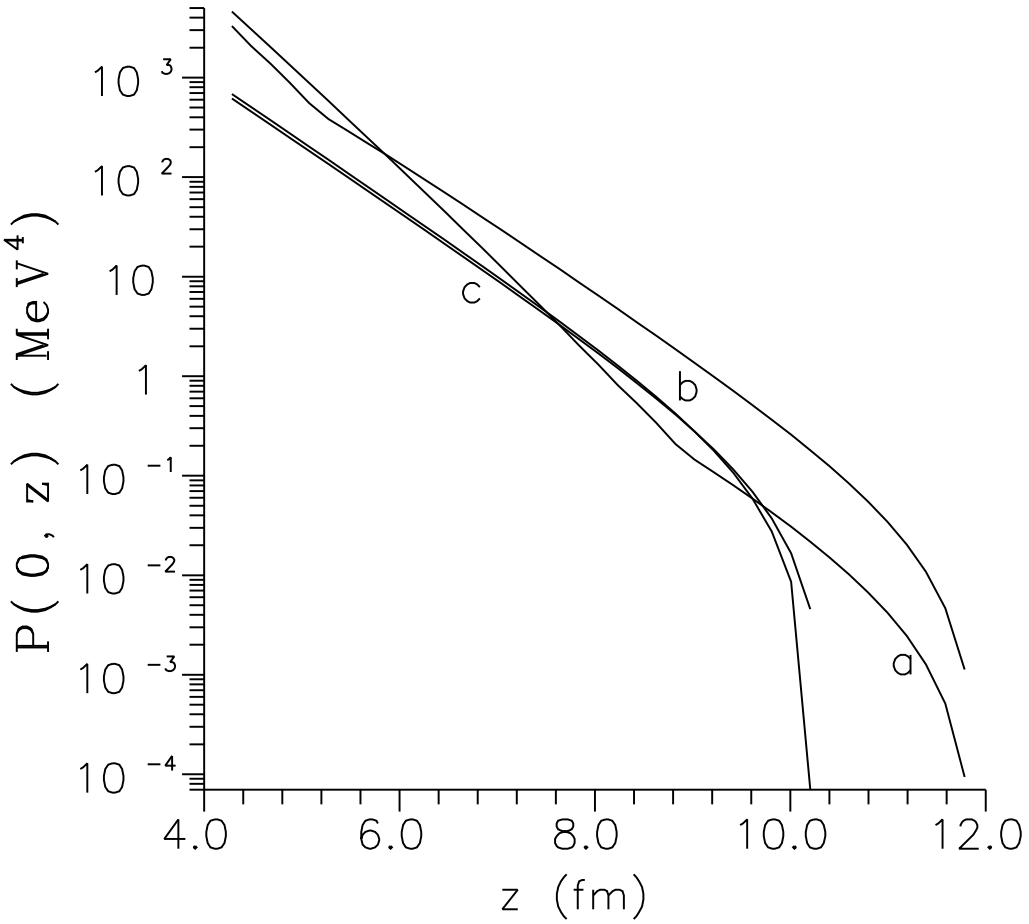

Fig. 15. The variation of kinetic pressure of non-uniform electron gas within WS cell with the axial coordinate in Fermi. Curves a and b are for $B = 10 \times B_c^{(e)}$ and $5 \times 10^2 B_c^{(e)}$ respectively, whereas upper and the lower curves indicated by c are for $5 \times 10^3 B_c^{(e)}$ and $10^4 \times B_c^{(e)}$ respectively.

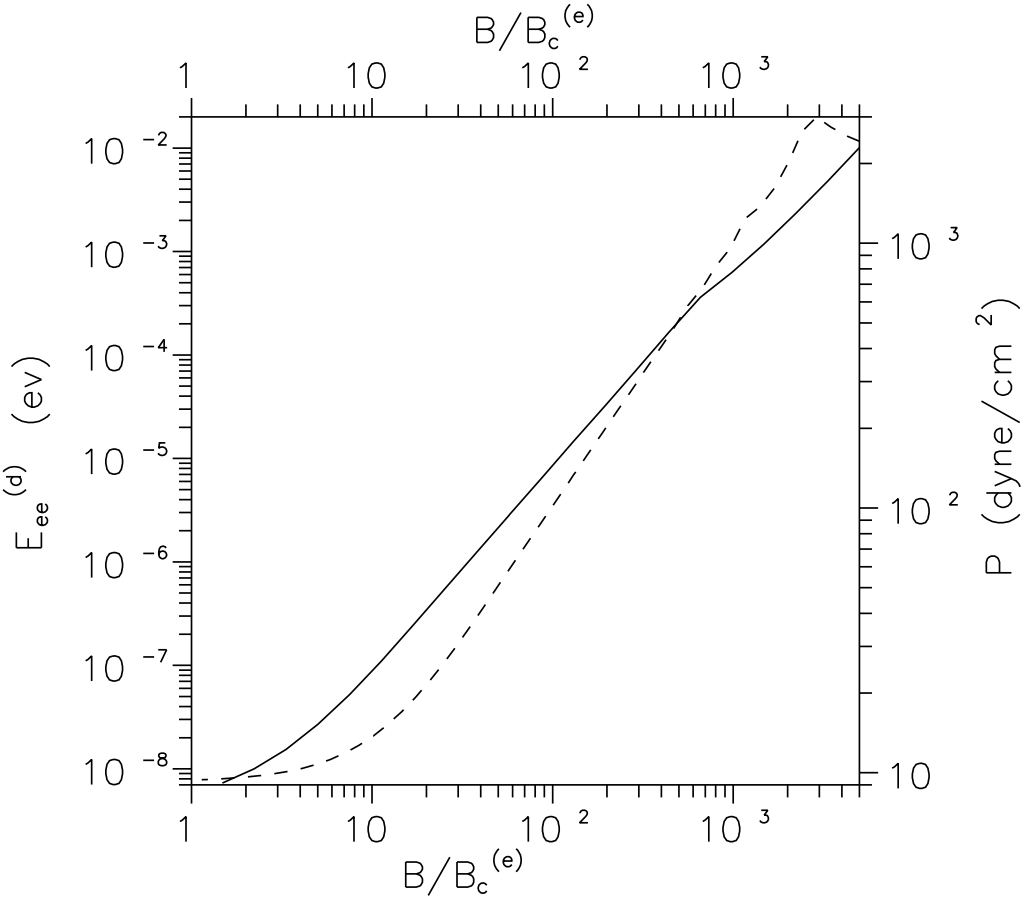

Fig. 16. The variation of cell averaged electron-electron direct interaction energy in ev (solid curve) and the cell averaged electronn kinetic pressure (dashed curve) with the strength of magnetic field.

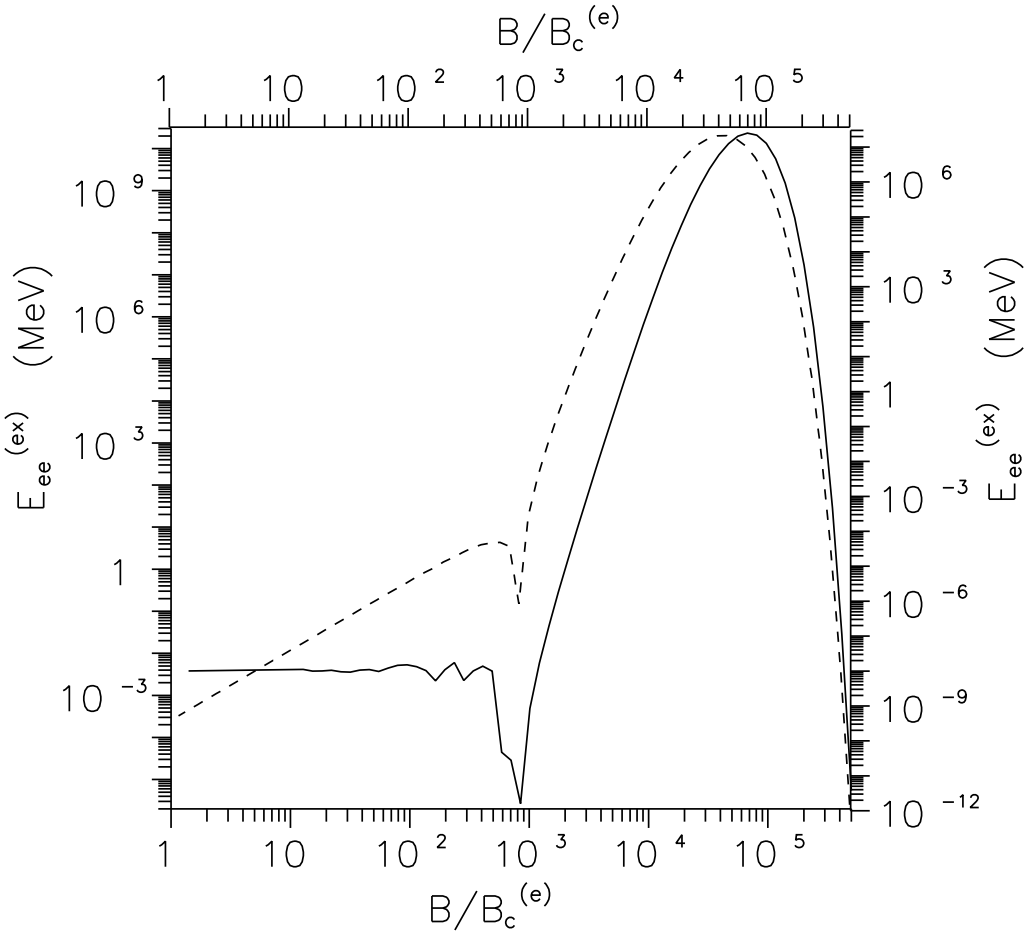

Fig. 17. The variation of cell averaged magnitude of the electron-electron exchange energy for $\nu \neq 0$ (solid curve) and the same quantity with $\nu = 0$ (dashed curve) with the strength of magnetic field.

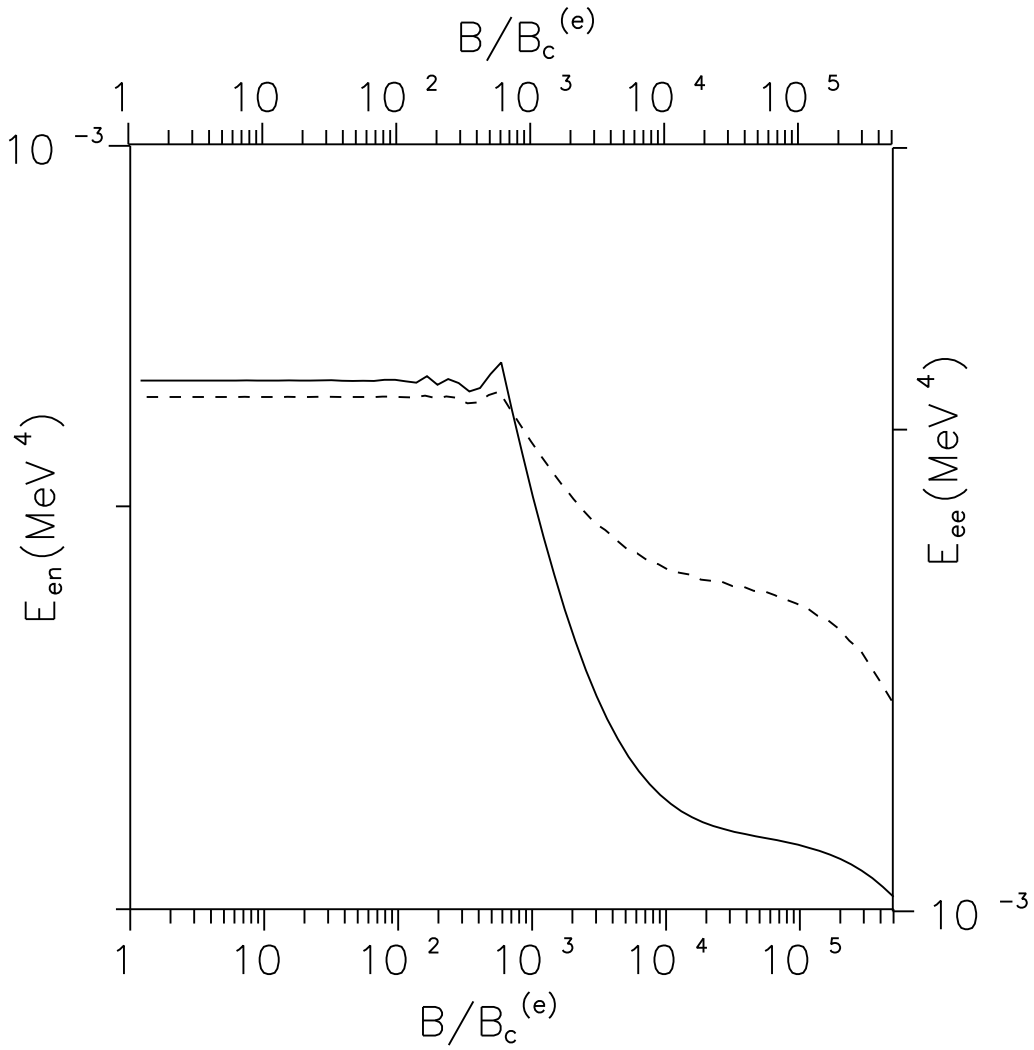

Fig. 18. The variation of cell averaged electron-electron Coulomb energy density (solid curve) and electron-nucleus Coulomb energy density (dashed curve) with the strength of magnetic field.

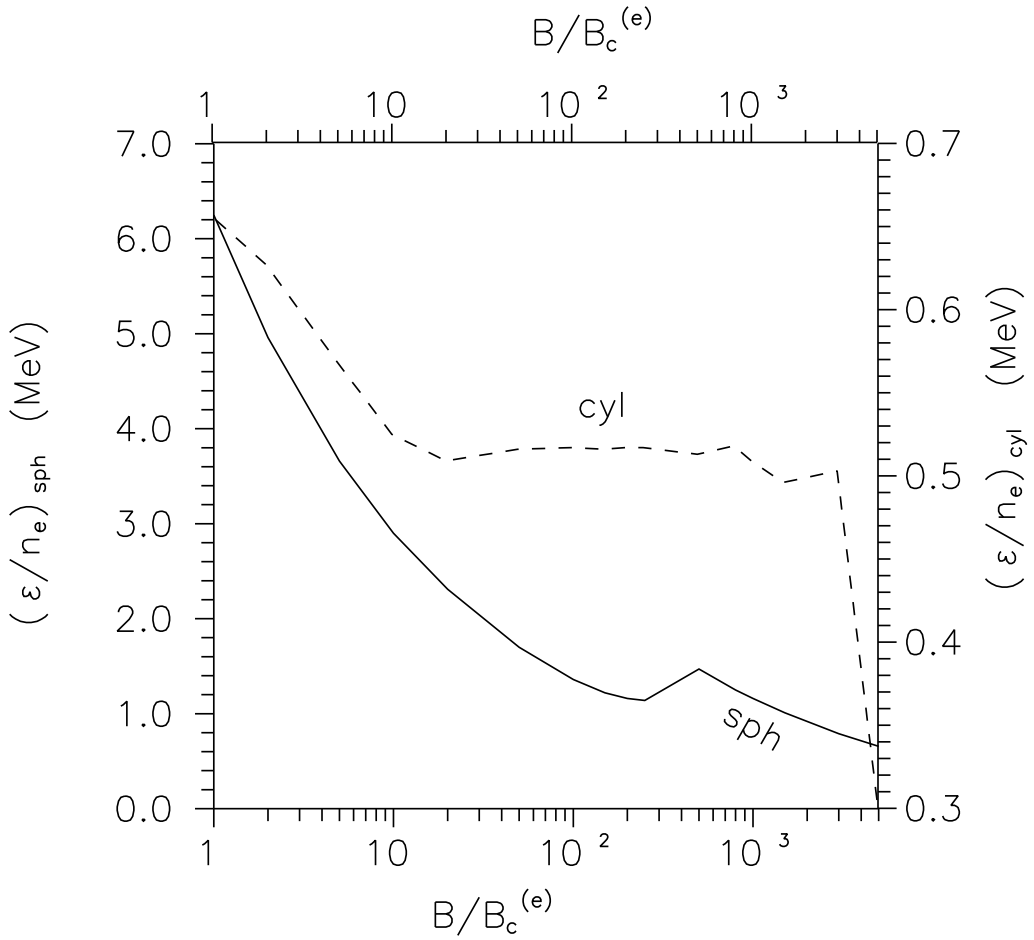

Fig. 19. Variation of total energy per electron in MeV with the strength of magnetic field. The solid curve is for the spherical case with energy per electron plotted along left y-axis and the dashed one is for the cylindrically deformed case with energy per electron plotted along right y-axis.